University of Alberta

VO_x/TiO_2 anode catalyst for oxidation of CH_4 containing 5000 ppm H_2S in SOFC

by

Alfonso Andrés Garcia Rojas

A thesis submitted to the Faculty of Graduate Studies and Research
in partial fulfillment of the requirements for the degree of

Master of Science
in
Materials Engineering

Department of Chemical and Materials Engineering

Abstract

In this research, $LSB_{10}T$/YSZ composite anode with VO_x/TiO_2 is used to improve the electrochemical performance, coking resistance and sulfur tolerance of high temperature SOFC fed by 5000 ppm H2S containing methane.

The ionic and electronic conductivities of $La_{0.4}Sr_{0.5}Ba_{0.1}TiO_3$ were studied with blocking electrodes. Sintering at reducing conditions leads to an increment of the total and electronic conductivity due to reduction of the oxidation state of Ti. On the other hand, sintering at oxidizing conditions increases the ionic conductivity due to the effect of barium on the enlargement of the free volume of the perovskite. Nonetheless, despite of this increment, the electronic conductivity prevails. When $LSB_{10}T$ was impregnated inside a porous YSZ matrix, an electronic conducting layer made of $LSB_{10}T$ covers the matrix, impeding the normal migration of oxide ions.

SOFC using hydrocarbon fuels suffer from carbon deposition on the surface of the anode and poisoning of the catalyst. Eventually, this deposition accelerates the degradation of the anode and decreases the overall electrochemical performance of the cell. For this reason, catalysts with high oxidizing activities are needed to avoid the formation of free carbon and further deposition.

In attempt to improve the activity of the composite anode, $LSB_{10}T$ /YSZ, small concentration of VOx/TiO_2 was infiltrated. VO_x/ TiO_2 exhibits good activity

for oxidation of sour gas and methane without detectable sulfur deposition or sulphidation. Furthermore, the TiO_2 enhances thermal stability of the active phase VO_x, ascribed to the relative electronegativity and affinity between the active phase and the support. Radiographic characterization shows that the active phase, VO_x comprises mainly vanadate entities. The enhancement on the catalytic oxidation of hydrocarbons conducts to high power density and low polarization. Finally, the presence of VOx/TiO_2 inside the composite anode $LSB_{10}T$ /YSZ enhances the electrochemical performance of the SOFC, the coking resistance of the anode, keeping the good sulfur tolerant of the composite.

Acknowledgements

I would like to thank my parents and siblings for supporting me to attain my masters and for their unconditional love, especially my mom who has been the main source of strength and encouraged me to make the most of this experience.

I am also very grateful to my supervisor, Jingli Luo, for her advice, support, guidance and offering me the unique opportunity to be part of this research group and study in this amazing country and university.

I want to express my gratitude to my research group and friends for our helpful discussions, and their company. They made this experience so joyful, full of beautiful memories and moments. Similarly, I want to thank all my Professors and CME administrative staff who have shared their knowledge and thoughts in making my academic experience so valuable.

I would like to specially thank, Muriel Stanley Venne, the first and most special person that I've met in Canada. She kindly hosted me at her home and adopted me as her son to make my adaptation in this country a more pleasant experience.

Finally, I want to acknowledge to Dr. Vincent for his mentoring during the first part of this research project and members in our Fuel Cell and Corrosion group, Dr. Singh and Dr. Hill for our valuable group collaboration and the NSERC Solid Oxide Fuel Cell Canada Strategic Research Network for supporting

us financially and giving me the opportunity to travel around Canada attending to

research meetings to broaden my knowledge.

Table of Contents

List of Tables

List of Figures

List of abbreviations

AFC	Alkaline fuel cell
BE	Blocking electrodes
EIS	Electrochemical impedance spectroscopy
EMF	Electromotive force
FTIR	Fourier Transform Infra-Red Spectroscopy
GDC	Gadolinium doped ceria
LDC	Lanthanum doped ceria
$LSB_{10}T$	Barium doped lanthanum strontium titanate ($La_{0.4}Sr_{0.5}Ba_{0.1}TiO_3$)
LSBT	Barium doped lanthanum strontium titanate
LSC	Strontium doped lanthanum chromate
LSM	Lanthanum strontium manganese
LST	Lanthanum strontium titanate
LSV	Lanthanum strontium vanadate
MCFC	Molten carbonate fuel cell
MEA	Membrane electrode assembly
MIEC	Mixed ionic and electronic conductor

OCV	Open circuit voltage
PEMFC	Polymer electrolyte fuel cell
PMMA	Polymethylmethacrylate
SDC	Samarium doped ceria
SEM	Scanning electron microscope
SOFC	Solid oxide fuel cell
SSZ	Scandia stabilized zirconia
TEC	Thermal expansion coefficient
TPB	Triple phase boundary
TPO	Temperature programmed oxidation
XPS	X-ray Photoelectron Spectroscopy
XRD	X-Ray Diffraction
YSZ	Yttrium stabilized zirconia

List of Symbols

α	Geometry factor
ASR	Area specific resistance
C_{bulk}	Concentration at the bulk
C_S	Concentration at the interface
d	Thickness of the diffusive layer
E_{eq}^o	Standard equilibrium potential
E_{eq}	Equilibrium potential
E	Cell potential
F	Faraday's constant
ΔG^o	Standard Gibbs free energy
ΔG	Gibbs free energy
ΔH^o	Standard Enthalpy
i	Net current density
i_o	Exchange current density
i_L	Limiting current density
σ	Dense sample conductivity

σ_{porous}	Porous sample conductivity
R	Electrical resistance
N	Efficiency
n	Number of electrons
η_{act}	Activation polarization
η_{con}	Concentration polarization
η_{ohm}	Resistance polarization
R	Gas Constant
ΔS^o	Standard Entropy
T	Temperature
v	Number of moles
v_v	Volume fraction porosity

Chapter 1   Introduction

1.1   Gas fuels

Fossil fuel, organic component formed by natural processes, has been the most predominant energy and power source in the last decades [1]. For this reason, our society has relied on this kind of fuel to deliver energy around the world leaving behind other type of energy sources such as nuclear power and renewable power sources including hydroelectric power, solar power, wind power and biofuel.

Coal, liquid oil and gas are fuels derivative from fossil fuel extracted from reservoirs in form of solid, liquid and gas state, respectively. However, liquid oil is the desirable fuel among fossil fuels due its chemical state, easy transportation, treatment, reforming and relatively high profitability [1].

Figure 1-1 shows the consumption of different fuels for the last 60 years and projects their consumption in the near future. Based on this projection, it is clear that the demand of liquid oil will increase forcing to look for alternative fuels and power resources. Then, due to the current availability of coal and gas, they seem to be good alternative and feasible options to replace the liquid fuel in the future.
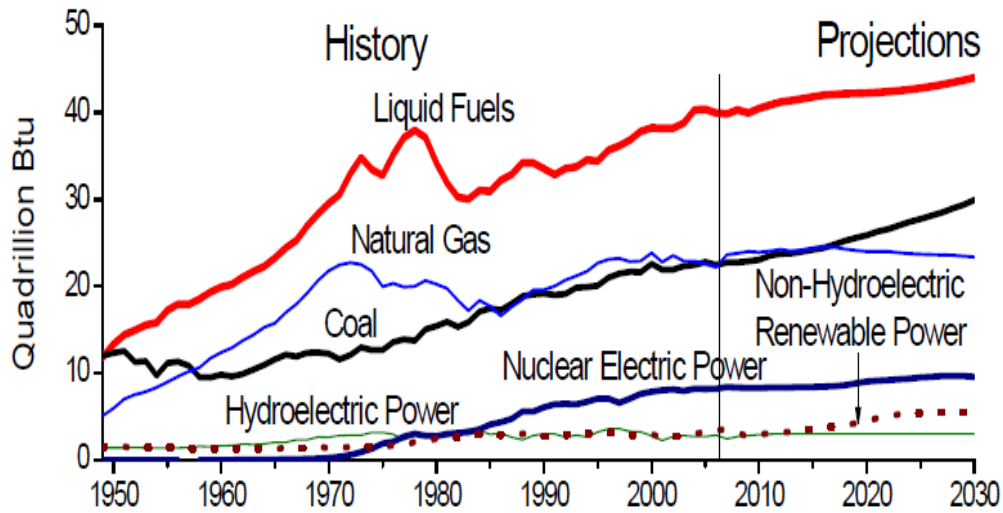
Figure 1-1 The world energy consumption history and outlook [2]

On the other hand, the use of fossil fuels leads to considerable CO_2 and greenhouse gas emission from the fuel combustion resulting in health and environmental issues such as global warming [3-8]. This emission is even worse considering the low fuel efficiency in engines, less than 40%, and high volumes of reactant needed to combust. In this process, the energy is partly wasted or lost in form of heat that flows to the surroundings, limiting the useful work and power output from combustion of the fuel. In addition to this poor efficiency, higher flow of fuel is needed to meet the power output requirements falling into more production of toxic gases and CO_2 emission.

In attempt to produce less toxic gases and increase the efficiency of energy conversion, hybrid and regular fuel cells have been introduced [9, 10, 10]. Rather than engines which use direct combustion reactions to produce work and energy, fuel cells use electrochemical reactions as main mechanism for energy

2

conversion. The fuel cells exhibit higher efficiencies than engines and lower CO_2 emission, reducing it by almost 60% [11]. In addition, fuel cells have been fuelled with liquid oil, coal and gas and become an attractive alternative due to its ability to utilize other type of gases usually considered as disposables or hazardous.

Fuel cells can utilize a variety of gases such as hydrogen, natural gas and sour gas. Hydrogen is easily produced by either electrolysis of water or steam reforming, increasing its availability. Regarding its performance as a fuel, hydrogen is very reactive, easy to oxidize and environmentally friendly [9, 11, 12]. However, the volatility of this element still imposes challenges in the storage of the fuel and safety restrictions limiting its application to specific sectors.

Natural gas is not as reactive and ecologically volatile as hydrogen and its availability makes this compound one of the most utilized gases, especially in the transportation sector [13]. Through combustion reactions, high amount of energy is released and partially converted in either work or electricity to produce power. In fuel cells, natural gas can be reformed or humidified to promote water shift reactions increasing the oxygen to carbon ratio and decrease the concentration of free radical of carbon that may poison the catalyst of the fuel cell. Also, some fuel cells with carbon tolerant catalyst have used methane or natural gas with very low content of water and low reforming or without previous reforming under dry conditions with relatively good success and performance [14]. This is the case for ceria based catalysts which have been used in solid oxide fuel cells [15].

3

Sour gas or methane containing H_2S is not usually used as fuel because of the detrimental effect of H_2S which is considered hazardous and corrosive, imposing a strict restriction on the direct fuelling of this gas [16]. For this reason, sour gas is sweetened to extract H_2S and further reformed to use the products as fuel [16]. In addition, due to the complexity of this reforming process and high cost, sour gas is the least desirable fuel gas among all the gases leading to lower demand and higher availability of the gas. Nowadays, with the higher efficiency of fuel cell and sulfur tolerant components that comprise some of them [17], the use of sour gas as fuel starts to be considered as a viable option to replace other fossil fuels and a more economical option to fuel these cells.

1.2 Fuel Cell principles

A fuel cell is an electrochemical device that transforms the chemical energy strode in a fuel into electric energy [10]. Rather than batteries, which only supply electric energy from the stored reactants, fuel cells can supply electricity as long as the fuel and oxidant are delivered to the electrodes. The main components of the fuel cell are the electrodes, cathode, anode, and electrolyte, which are assembled together and known as membrane electrode assembly (MEA), as shown in Figure 1-2.

4
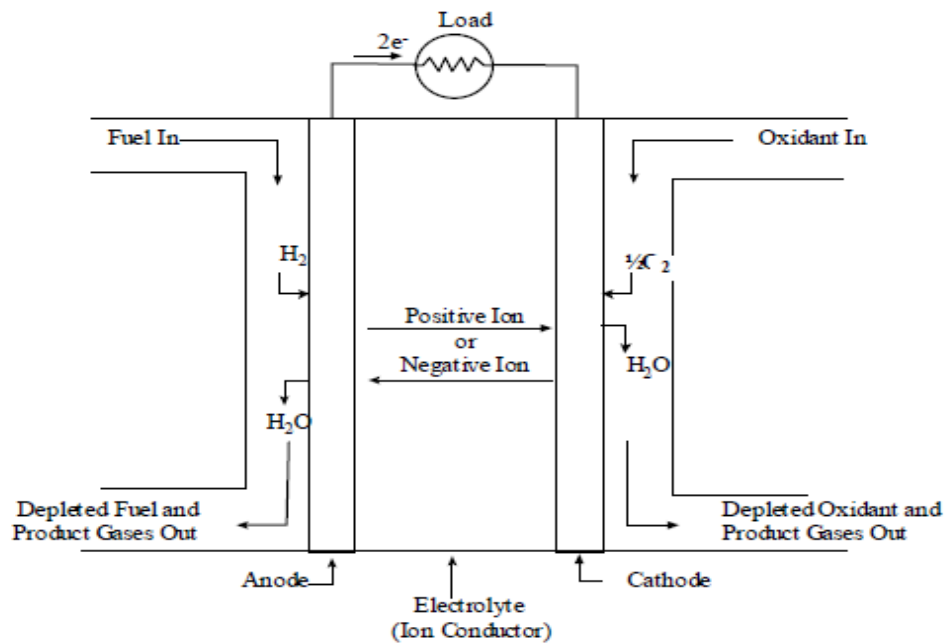
Figure 1-2 Schematic of a membrane electrode assembly (MEA) [18]

The electrolyte has to be dense to prevent gas cross over and a pure ionic conductor to transport ions from electrode to electrode preventing the conductivity of electrons which drops the open circuit voltage, voltage at equilibrium conditions, and leads to short circuit [10]. Depending on the properties and composition of the electrolyte they may transport different ions, positive or negative ions, and alter the electrochemical reaction mechanism of the fuel cell.

When a positive ionic conducting electrolyte is used, the fuel is catalytically decomposed on the surface of the anode producing electrons and positive ions which are transported by the action of the electric field and different potential at the electrodes [19]. The ions are conducted along the electrolyte, and

the electrons through the current collectors that are usually made of metal with predominant electronic conductivity. The migration of ion and electrons makes them to meet at the cathode and electrochemically react with the oxidant. Similarly, when a negative conducting electrolyte is used, the oxidant reacts at the cathode and reaction product is negatively charged by the transported electrons through the current collector [20]. The electric field, polarization and conducting components, transport the ions along the electrolyte. The negative ions oxidize the fuel electrochemically at the anode site, completing the reaction. Currently it is known OH^-, O^{2-}, CO_3^{2-} and H^+ conducting electrolytes for different fuel cells [18].

The electrodes comprise an important element of the fuel cell and an important role carrying out all the electrochemical reactions in presence of a catalyst. At the anode, electron generation and oxidation of the fuel take place while at cathode, the electrons are consumed and oxidant is reduced [10]. The electrodes are porous to make the gas to diffuse inside the microstructure, with a large surface area to promote electrochemical reactions and affinity to allow physical or chemical adsorption and intimate contact of the reactants [10]. In addition, the electrodes are mixed ionic and electronic conductor (MIEC) to transport charged species coming from the electrolyte and electrochemical decomposition of the reactants.

The sites where the electrochemical reduction or oxidation reactions take place are known as triple phase boundaries, TPB, and maximization of these sites lead to higher current and power density output of the fuel cell [21-24]. For these reasons, materials with low particle size in a range of nanometers with good ionic,

6

electronic conductivities and catalytic activity are highly desired [25]. Figure 1-3 describes a typical scheme of electrochemical reduction of oxygen at TPB at the cathode side and subsequent transfer of oxygen ions along the electrolyte.
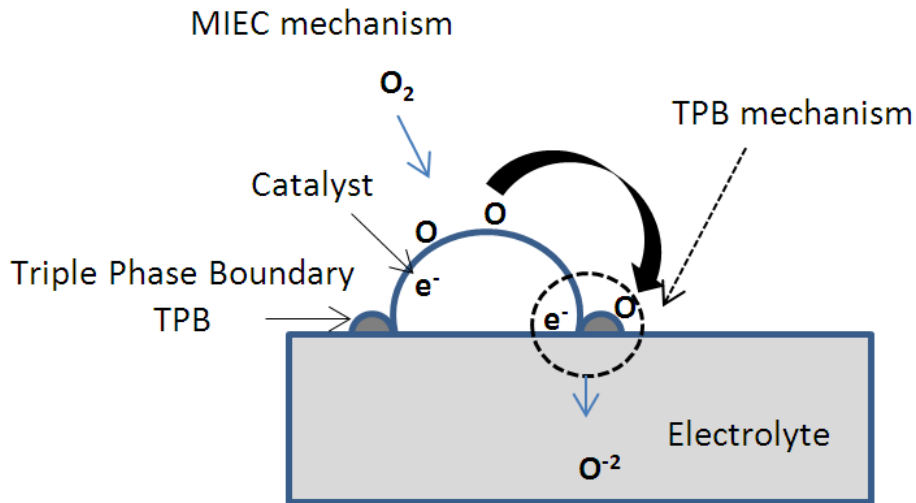
Figure 1-3 Schematic mechanism of TPB [26]

1.3 Fuel Cell thermodynamic principles

In a process involving energy transformation and exerted work are governed by thermodynamic principles and fuel cell is not an exemption. The available energy to produce a work can be expressed in term of Gibbs free energy, ΔG, which depends on the entropy, ΔS, and enthalpy, ΔH or heat potential, intrinsic properties of the component in an open system [10]. Entropy tends to increase, disorder, decreasing the energy that can be efficiently converted in work.

For an isothermal process, first law of thermodynamic can be express according to Equation 1-1, which point out energy conservation:

$$\Delta G^o = \Delta H^o - T\Delta S^o \qquad\qquad \text{1-1}$$

where $\Delta G^o, \Delta H^o, \Delta S^o$ are the standard Gibbs free energy, standard enthalpy and standard entropy, respectively, calculated at standard conditions, temperature **T**= 25°C.

For a system with more than one electro active species, the Gibbs free energy can be rearranged and expressed in terms of the chemical potential and activity of the species. By setting a reference point, usually at standard conditions 1 atm and 25°C, $\boldsymbol{\Delta G^{\circ}}$ is calculated and the free energy $\boldsymbol{\Delta G}$ is expressed by Equation 1-2:

$$\Delta G = \Delta G^{\circ} + RT \ln \frac{a_{product}^{v_i}}{a_{reactant}^{v_i}} \qquad\qquad \text{1-2}$$

where $\boldsymbol{R}$ is the gas constant, $\boldsymbol{a}$, the activity of the species that participates in the reaction and $\boldsymbol{v_i}$, the stoichiometric value of the species.

The free energy can be also linked to the electrical potential, E, by introducing the Nernst equation which is expressed in Equation 1-3:

$$\Delta G^{\circ} = -nFE^o{}_{eq} \qquad\qquad \text{1-3}$$

where $\boldsymbol{F}$ is the Faraday's constant, $\boldsymbol{n}$ is the number of electrons involved in the electrochemical reaction, and $E^o{}_{eq}$ is the equilibrium potential calculated at standard conditions. Combining Equations 1-2 and 1-3, the electrical potential is expressed in terms of the activities of the electro active species [27]:

8

$$E_{eq} = E^o{}_{eq} - \frac{RT}{nF} ln \frac{a^{v_i}_{product}}{a^{v_i}_{reactant}} \qquad \textbf{1-4}$$

where E_{eq} the equilibrium is potential calculated at the non-standard condition.

Considering that the enthalpy is the total energy stored in an open system and the Gibbs free energy is the available energy that can be used to produce electric work in a fuel cell, the ideal fuel cell efficiency, N, is defined as the ratio of the free energy to the total enthalpy and is given by Equation 1-5:

$$N = \frac{\Delta G}{\Delta H} = -\frac{nFE_{eq}}{\Delta H} \qquad \textbf{1-5}$$

However, the practical efficiency in fuel cell is not close to the theoretical efficiency owing to energy losses or potential drops arising from sluggish electrochemical reactions, high resistivity or poor diffusivity and delivering of the fuel and oxidant at the electrodes.

1.4 Fuel cell polarization

As mentioned, fuel cell has energy losses coming from overpotentials or potential drops. To have a better understanding of these losses, the kinetics of the electrochemical reaction, transport phenomena and ohmic resistance should be considered. Three main loss sources or polarizations have been identified, activation, resistant and concentration over voltages [10].

In the activation polarization, sluggish electrochemical reactions reduce charge transfer at the anode and cathode, polarizing the electrodes [28, 29]. To decreases this type of polarization, good catalysts are used at the electrodes to rapidly reduce or oxidize the delivering gases as well as maximizing the reaction points, TPB, to increase the current density. For high temperature fuel cells such as solid oxide fuel cell, SOFC, high temperatures lead to faster electrochemical reactions and lower activation polarization. For this reason, the activation polarization is rather low for SOFC and can be expressed linearly as depicted by Equation 1-6:

$$\eta_{act} = \frac{iRT}{nFi_o} \qquad\qquad 1\text{-}6$$

where η_{act} is the activation polarization, i the current density and i_o the exchange current density.

The resistant polarization, another sort of over polarization, is product of the not proper conduction of charge species producing heat dissipation and impeding the normal flow of the current. The conductivity depends on the electric field, mobility of charge, concentration of the charge carriers these last two variables are material properties.

Regarding the mobility of the charge carriers, electrons and ions, due to its larger size the ions move slower than electrons do hampering the normal flow of the current. For this reason, most of the ohmic loss comes from the poor ionic conductivity of the electrolyte and thin electrolyte are preferred to reduce this loss [10]. For example, the polymer exchange membrane fuel cell, PEMFC, uses a

10

thin and conducting polymer as electrolyte to reduce this loss, unlike SOFC which uses component with relatively good mechanical properties but low conductivity, such as ceramics, under its operating conditions, making this kind of polarization a considerable loss source [30, 31]. Furthermore, resistances and losses may also come from current collectors and at the interface of the MEA, these losses may be considered as minor compared to those that come from the electrolyte. Equation 1-7, known also as ohms' law, expressed the resistance polarization in term of the current density:

$$\eta_{ohm} = i * ASR \qquad \text{1-7}$$

where η_{ohm} is the resistance polarization and ASR is defined as the area specific resistance of the cell.

Finally, the concentration polarization is referred to mass transfer, poor diffusivity of the reactant that cannot reach deeper inside the electrodes, developing concentration gradient and leading to concentration polarization loss [32]. Using the Fick's law, the current and limiting current density defined as the maximum current yield due to the complete consumption of reactants, is expressed in terms of the gas diffusivity and concentration gradient, and given by Equations 1-8 and 1-9:

$$i = \frac{nFD \; C_B - C_s}{d} \qquad \text{1-8}$$

$$\lim_{C_s \to 0} i \; = i_L = \frac{nFDC_B}{d} \qquad \text{1-9}$$

where D is the diffusion coefficient, i_L is the limiting current density, C_b concentration of the specie at the bulk, C_s the concentration of the specie at the interface and d is the thickness of the diffusion layer.

Finally, using the two expressions above, the concentration polarization is expressed by Equation 1-10:

$$\eta_{con} = \frac{RT}{nF} ln \left(1 - \frac{i}{i_L} \right) \qquad \textbf{1-10}$$

where η_{con} is the concentration polarization.

The voltage of the cell is deviated from the equilibrium potential and these three types of polarizations and is given by Equation 1-11:

$$E = E_{eq} - \eta_{act} - \eta_{ohm} - \eta_{con} \qquad \textbf{1-11}$$

where E is the voltage of the cell.

Usually at high voltages and low current densities, the activation polarization and electrochemical reaction is the limiting step. At intermediate voltages, the resistance polarization turns out to be the limiting step while and at low voltages and high current densities, the reactants are consumed rapidly and the gas does not have enough time to diffuse to the TPBs, resulting in concentration gradients. Under this condition, the concentration polarization also causes significant voltage loss.

1.5 Types of fuel cells

Currently, there are different kind of fuel cells which are classified by type of electrolyte and their ionic conducting mechanism. They are the polymer electrolyte fuel cell (PEFC), alkaline fuel cell (AFC), phosphoric solid oxide fuel cell (PAFC), molten carbonate fuel cell (MCFC), and the SOFC. These conducting mechanism and electrolytes allows the fuel cell to operate at different temperatures and with different fuels, hydrogen, natural gas, syngas or sour gas.

PEFC uses a polymer ion exchange membrane as electrolyte conducting only H^+ ions from the anode to the cathode side [19, 33]. At the anode, hydrogen is delivered and catalytically decomposed to produce H^+ and e^- at around 100°C or lower. Platinum is used as catalyst due to the good catalytic activity exhibited at the operating temperatures of the fuel cell [10]. Nonetheless, the use of this catalyst imposes a restriction on the application of syngas, natural gas and sour gas due its easy deactivation and sulfur and carbon poisoning. In addition, the polymer membrane should be hydrated to keep the conductivity of protons limiting the operating temperature range, lower than 100° C to prevent the evaporation of water but higher than 80° C to promote the oxidation of the fuel.

AFC has an electrolyte that is made of alkaline solution, potassium hydroxide, impregnated in a matrix of asbestos, conducing OH^- ions form cathode side to the anode side [20]. Depending on the concentration of the alkaline solution the operating temperature of the fuel cell may vary but usually operates from 70°C to 90°C [10]. Since the alkaline solution might react with hydrocarbon

13

forming some undesirable side products which decrease the ionic conductivity of the electrolyte, the fuel is restricted only to hydrogen.

PAFC might be injected with either H_2 or syngas with low concentration of carbon monoxide to avoid poisoning of the catalyst, platinum. The electrolyte consists in concentrated phosphoric acid able to conduct H^+ ion along from the anode to the cathode side [34]. The operating temperature range from 150 to 220 °C but it is preferable to operate at higher temperature conditions to enhance the ionic conductivity of the electrolyte and avoid CO poisoning [18].

MCFC could be fueled with hydrogen or syngas using a membrane made of alkali carbonate membrane contained in a ceramic electrolyte $LiAlO_2$ which conducts CO_3^{2-} from the cathode side to the anode side [35]. The cell can operate from 600 to 700 °C and uses nickel rather than platinum as catalyst due to its higher resistance to CO poisoning exhibited at these conditions [18]. However, the electrolyte is corrosive and the fuel cell has to use a recycling system to efficiently deliver CO_2 from the anode to the cathode side to produce ion CO^{3-} and enhance the conductivity of the membrane.

Special attention has been addressed to SOFC lately. This cell has been fueled with lot of kind of gases including syngas, natural gas, sour gas and H_2. Its electrolyte is ceramic, metal oxides, and the most common one is yttrium stabilized zirconia abbreviated and commonly known as YSZ which is able to conduct O^{2-} ions. The high temperature range, from 700 to 1000°C, becomes in an

important variable to promote faster electrochemical reactions, therefore less expensive metals can be used as catalysts at low concentration [36].

1.6 Solid oxide fuel cell

The possibility to operate a SOFC at a high temperature range brings some benefits reflected on higher power output, efficiency of the cell and energy conversion as well as fast electrochemical reactions [37]. In addition, at these conditions there is a notorious improvement on the reactivity of the fuel leading to easier electrochemical oxidation reactions and possible application of natural gas and syngas considered as inactive at low temperature for fuel cells. The possibility to use less expensive fuels makes this cell to stand out and decrease significantly fuel cell operating cost [17].

On the other hand, at high temperatures materials are subjected to high mechanical stress and undesirable chemical reaction that may alter their properties and limits the material selection for fuel cell applications. For example, the application of many metals in high temperature SOFC is rather considered unrealistic considering that they can be easily poisoned with carbon and sulfur or corroded, resulting in a high material instability [38, 39]. Similarly, some metals in reducing condition may become brittle losing most of their good mechanical properties [40]. For this reason, mechanical properties and stability have become important criteria for material selection. Stable metal oxides are the more practical material for SOFC application due to their good mechanical and chemical stabilities under operating conditions but its conductivity and activity has to be

15

greatly improved. Ceramics comprise the framework of high temperature SOFC since they are not easily oxidized and corroded at high oxidizing conditions despite of the high temperatures at which they are exposed [10]. Beside this material, unlike metals, exhibit ionic and electronic conductivity, and their conducting properties can be easily tailored by doping extra elements to get higher ionic conductivities and similar electronic conductivity exhibited by some metals [41]. This behavior allows designing and enhancing the TPB to maximize the electrochemical reaction [21, 23, 42]. Figure 1-5 shows the area of electrochemical reactions and TPB when electronic, ionic or mixed electronic ionic conductors, MIEC, comprises the electrode.
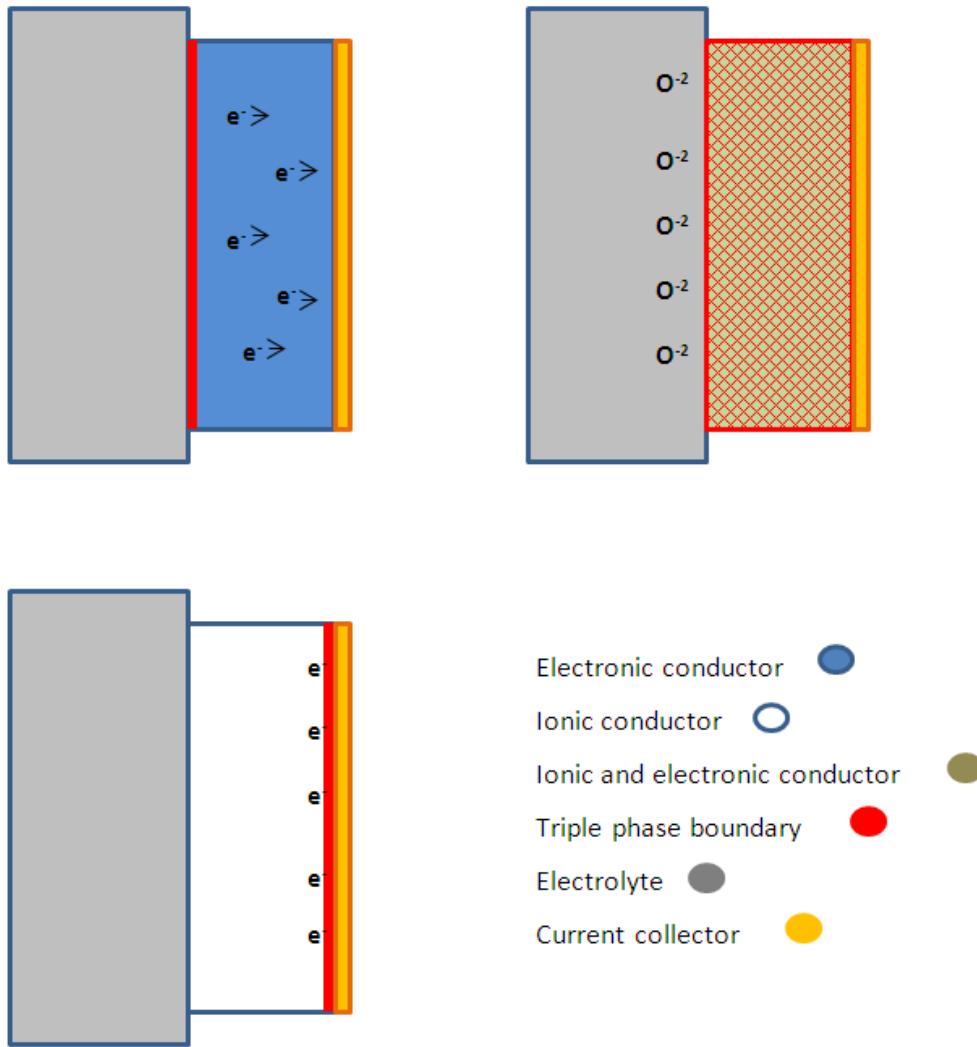
Figure 1-4 Scheme showing different TPB [42]

Nonetheless, high temperatures promote thermal expansion mismatches and undesirable reactions among the materials leading to new components with poor properties. For this reason, composite electrodes are desirable having components with similar thermal expansion coefficient (TEC) to avoid cracks as well as stable compounds with low reactivity among them [43].

Additionally, the material should exhibit specific activity to foster the desirable reactions with the gas and avoid reactivity and side reactions that might poison or degrade the material. For example, thermal cracking of methane lead to severe carbon production and the deposition of the carbon on the surface deactivates the catalyst and causes poor conductivity blocking the conduction of electrons and ions. Beside, when methane contains H_2S, other detrimental effect of the gas may arise from the presence of H_2S [44]. At low concentration of H_2S there is high production of sulfur and further deposition of this element on the surface of the anode, poisoning the anode catalyst [38]. At high concentration, the sulfur reacts with the anode, degrading this last component of the cell. Hence, main challenge relies on the improvement of the composite electrodes, especially on the composite anode which is exposed to these gases.

The MEA makes reference to the structure of the fuel cell and how the electrolyte, anode and cathode are assembly. Then, fuel cell can be either supported by a thick anode, thick cathode or electrolyte and may exhibit two conventional geometries of the MEA, planar and tubular.

Electrolyte supported fuel cell usually uses YSZ electrolyte with a thickness of around 100μm and thin electrodes [10, 18]. This configuration enhances the diffusivity of the oxidant and fuel through the porous electrodes but presents high ionic resistance at the electrolyte. Depending on the type of conductivity of the electrolyte, higher operating temperatures might be needed to increase the ionic conductivity and reduce the resistance of the electrolyte.

Electrode supported fuel cell has either a thick anode or cathode. In this configuration, the electrolyte is about 5-10µm thinner that in electrolyte supported cells, reducing ohmic losses of the cell considerably and increasing the power output [18]. Though, in this configuration the diffusivity of the gases has to be improved by optimizing porosity of electrodes and getting a nice microstructure with conducting channels to improve the delivering of the active gases to the TPB and close to the electrolyte.

Cathode supported cell made of a mixture of YSZ and lanthanum strontium manganese, LSM is commonly used owing to their similar TECs of cathode and electrolyte. Having similar TEC allows fuel cells with thinner electrolytes preventing cracks and gas cross over. Figure 1-6 depicts electrolyte and anode support configurations of planar SOFCs.
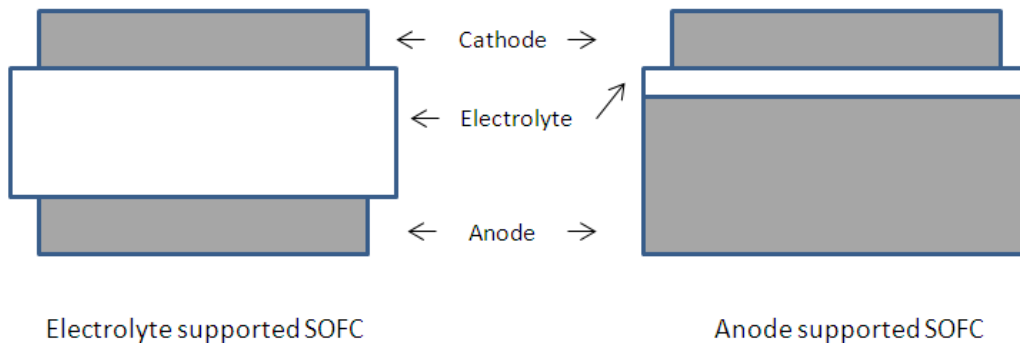
Figure 1-5 Schemes of electrolyte and anode supported fuel cells [18]

Regarding the geometry of the fuel cell, the tubular configuration provides higher surface area and power density but technical issues concerning current

collectors limit the total power output of the cell [45]. Besides, the ohmic polarization of the cell is higher than that of planar configuration forcing to operate the tubular cell at high temperature range from, 900˚C to 1000 ˚C, to increase their conductivity. These operating conditions compared to the operating temperature of the planar configuration, 700 ˚C to 900 ˚C, makes the tubular cell a technically more complex configuration.

1.7 Solid oxide fuel cell anodes

At operating temperatures of the fuel cell, 700˚C to 1000 ˚C, the SOFC anodes suffer severe thermo mechanical and chemical degradation. As an example, platinum, considered an active metal for the oxidation of hydrogen and excellent electronic conductor, at high temperatures it is not stable as it may degrade and becomes brittle in presence of hydrogen. Furthermore, when it is exposed to sour gas, such high temperatures crack the hydrocarbons and H_2S producing free radial of carbon and sulfur that block the active sites of the metal and poisoning it. Considering these risks and price of this metal, its application as anode for SOFC is not so feasible and economically profitable.

Another example is nickel, well-known SOFC anode and catalyst due to its wide application and good performance for oxidation of hydrogen. Though, this catalyst might be oxidized in presence of oxygen, its activity is still high enough to promote the dissociation of hydrogen and further oxidation and considered one of the most active metals [46]. Also, in presence of methane or syngas, carbon deposition is not as severe as it is with platinum or gold and some

studies have reported that the carbon deposition on nickel might be reduced adding copper due to the low catalytic activity of c-c bond formation of this second element [47]. Considering these factors, its availability and price, nickel imposes a more feasible application and profitable option for SOFC marketing.

Nickel has a poor ionic conductivity and needs to be mixed with a good ionic conductor to complete electrochemical reactions. Hence, this element is usually mixed with YSZ, this new composite is known as Ni/YSZ cermet, or impregnated inside a porous YSZ to increase the TPB and decrease the particle size of nickel to allow intimate contact between the gas, the ionic and electronic conductor. For this reason, the mixture ratio of Ni/YSZ plays an important role on the properties of the anode including the proper ionic, electronic conductivity and activity. Koide et al. stated that when the ratio Ni/YSZ increases the resistance of the anode decreases, and proposed an optimum ratio of 40/60 to decrease the polarization resistant [48].

In attempt to increase the ionic conductivity of nickel- cermet anodes, Ni/SSZ, scandia stabilized zirconia, has been studied. The addition of SSZ resulted in an enhancement of the ionic conductivity compare to the ionic conductivity exhibited by Ni/YSZ anodes [49]. Nevertheless, the application of Ni/SSY anodes is restricted but the high price of the SSZ imposing a restriction on the applicability of this anode in SOFC. Other composite anodes have also drawn the attention, one example is Ni-YDC, yttria doped ceria, where the presence of YDC seems to increase the rate of oxidation of hydrocarbon and

carbon monoxide. Therefore, Ni-YDC is a suitable catalyst for syngas fuelled SOFC [50].

Generally speaking, nickel-cermet anodes have shown a satisfactory performance for SOFC fuelled with hydrogen, methane or syngas but poor performance with high degradation rate when sour gas, methane containing H_2S, is used as fuel. Previously, it was mentioned that at low concentration of H_2S, below 20 ppm, the sulfur deposition on the surface of the anode is the main cause of poisoning. Even worse, on the surface of nickel, the sulfur deposition is irreversible at temperature range of 700 °C to 800°C due to high stability of the adsorption of sulfur on the metal [44, 49, 51].At high concentration of H_2S, adsorption of sulfur may occur but the sulphidation of nickel, reaction of nickel with sulfur, is mainly responsible for degrading and delaminating the anode from the MEA [49, 52, 53] .These drawbacks limit the application of this anode for methane containing H_2S fuelled SOFC. Therefore, alternative anodes with sulfur tolerance properties should be developed.

1.8 Anodes tolerant to sulfur

Usually SOFC anodes are very sensitive to any form of sulfur contained in unreformed fuels like H_2S [44]. This corrosive gas can poison the anode catalyst by either sulfur deposition or sulphidation of the anode at the operating temperature of the cell. For this reason, before delivering the fuel to the cell, the untreated gas is reformed, hydro treated or sweetened to remove any hazardous components [16]. Consequently, the previous treatment of the gas dramatically

raises the cost of the fuel and imposes an inability of using other more available gases. As a result, SOFC with sulfur tolerant anodes are desirable to use more available and economical fuel resources like sour gas or unreformed natural gas.

Some metal sulfides, products of oxidation of H_2S with metals, have surprisingly shown acceptable stability and performance in SOFC. Among all the metal sulfides, $NiFe_2S_4$, WS_2 and $CuCo_2S_4$ are considered the most actives anodes [49]. Their primary catalytic activity resides on the H_2S decomposition to produce H_2 being H_2S oxidation, the second most favorable reaction. Despite of their good stability in H_2S, they are volatile at the operating conditions of the SOFC and some efforts have been focused on the stability of the metal sulfides at high temperatures. Nonetheless, it has been found that addition of nickel, platinum or copper increases the melting point of MoS_2 [49, 54].

Ceria and doped ceria oxides represent a new alternative for sulfur tolerant material. The availability of ceria makes it a cheaper material and a potential application for SOFC composite anodes. Ceria based materials are added to nickel cermet anodes to partially suppress the sulfur deposition on nickel. Sometime to further relieve the deposition of carbon and sulfur, cobalt is also added to the mixture. Recent study states that at around 450°C and 800°C sulphidation of ceria is likely and formation of CeO_2S_2 has been found decreasing the performance of the anode [49, 55]. On the other hand, gadolinium doped ceria oxide, GDC, improves the sulfur tolerance of ceria and increases the ionic conductivity of O^{-2} to reduce sulfur deposition and sulfidation and promoting SO_2 formation [49, 56]. Though, GDC exhibits a predominant ionic conductivity and

23

the electronic conductivity has to be greatly improved. Samarium doped ceria, SDC, also exhibit good activity but when it was mixed with Ni, sulfur poisoning was detected in the anode composite at equilibrium conditions [49, 57].

The applications of perovskite have called the attention due its good electrical conductivity that makes it a candidate for SOFC anode. In addition, perovskite are proven to be tolerant to H_2S and doping them with different elements, their conductivity, catalytic activity and sulfur tolerant can increase [49]. Even though, it is still hard to synthesize a perovskite that meets all the desirable properties, i.e., good conductivity, activity and H_2S tolerance [49]. For example, strontium doped lanthanum chromate, LSC, has a good stability in H_2S and good activity for oxidation reactions but its conductivity is low. When LSC is doped with manganese, the conductivity increase but its sulfur tolerance decreases [58]. Lanthanum strontium vanadate, LSV, is another perovskite with potential application in the SOFC due its good conductivity and good stability at high concentration of H_2S and performance. Unfortunately, its redox stability is low and it can be easily oxidized passing from $SrVO_3$ to $Sr_3V_2O_8$ which is a phase that acts as an insulator rather than a conductor [49, 59, 60].

Lanthanum strontium titanate, LST, is currently one of the most promising SOFC anode based on its high electronic conductivity and good stability at high concentration of H_2S [49]. Though its catalytic activity and ionic conductivity should be further improved, some studies have reported that by adding lanthanum doped ceria, LDC, sulfur tolerance can be further improved as well as the catalytic and ionic conductivity at high concentration of H_2S [49, 61].

24

The oxidizing activity of LST increases in some degree when it is doped with barium to produce LSBT, keeping the good electrical conductivity of the original LST [62]. Despite of this improvement, either LST or LSBT is intimately mixed with YSZ to increase the ionic conductivity. However, special attention is needed on increasing the catalytic activity of the composite anode.

1.9 Electrical conductivity of SOFC Anodes

Rather than a chemical catalyst an electrochemical catalyst with high ionic conductivity and good enough electronic conductivity is needed for SOFC anodes. Many components have been mentioned in this introduction but YSZ and LST are the more promising SOFC composite anodes so far. YSZ has a fluorite structure consisting of tetravalent cations, exhibiting a face centered cubic structure arrangement of cations with anions occupying tetrahedral sites [63]. To achieve higher oxide ion conductivity and introduction of oxygen vacancies, ZrO_2 is doped with yttrium, Y, a cation of lower valence. The dissolution of yttrium into ZrO_2 can be written by Equation 1-12 with the Kroger-Vink notation:

$$Y_2O_3 \; ZrO_2 \; \rightarrow 2Y'_{Zr} + 3O_o^x + V_o^{\bullet\bullet} \qquad \textbf{1-12}$$
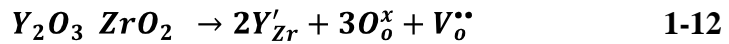
From Equation 1-12, it can be deduced that the concentration of oxygen vacancies is strongly dependent upon dopant level, concentration of yttrium. At low dopant levels, the oxide ion concentration increase linearly with the concentration of the dopant while at high dopant levels, the dopant starts to form clusters that reduce the ionic conductivity of the fluorite [63]. Nevertheless, at intermediate temperatures, YSZ exhibits low ionic conductivity making this

25

compound suitable for high temperature SOFC composite anodes rather than for intermediate temperature fuel cells.

Strontium titanate, SrTiO₃, is a perovskite with chemical structure ABO₃ and cubic structure with large-sized 12-coordinated cations at the A site and small-sized 6-coordinated cations at the B site [63]. This compound exhibits an n-type electronic conductivity at low partial pressure of oxygen reducing titanium to +3 which is the conducting form of this element. Equation 1-13 shows the conductivity mechanism of titanium oxide in reduced environment.

$$2Ti_{Ti}^x + O_o^x \rightarrow 2Ti_{Ti}' + V_{O}^{\cdot\cdot} + \frac{1}{2}O_{2(g)} \qquad \text{1-13}$$
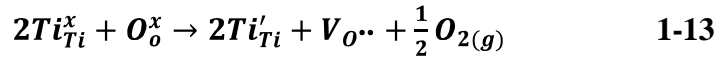
In attempt to increase its ionic conductivity, strontium is partially substituted with a cation of higher valance than lanthanum to enhance the ionic conductivity of the perovskite. Then to maintain charge neutrality, excess oxygen is introduced and can be expressed as interstitially and randomly localized defects [64], as given by Equation 1-14:

$$La_2O_3 + 2Sr_{Sr}^x \rightarrow 2SrO + 2La_{Sr\cdot}^{\cdot} + O_i'' \qquad \text{1-14}$$
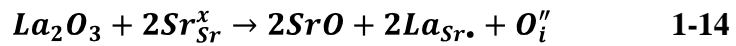
Even though, LST doesn't possess the desirable ionic conductivity for SOFC anodes, it turned out to be a good sulfur tolerant material with good electronic conductivity [65]. Another method to increase the ionic conductivity of LST is to increase the free volume and lattice parameter of the perovskite by doping with bigger cations at either the A or B site.

When LST is partially doped with barium at the A site of the perovskite and substituted strontium, the ionic conductivity might be further increased.

Vincent et al. doped LST with barium, Ba, to increase the catalytic activity and ionic conductivity of the LST [62]. Though, the ionic conductivity was not formally measured, LSBT exhibited higher activity than LST. Despite of this improvement, LST or LSBT still needs to be intimately mixed with YSZ to increase the ionic conductivity and TPB. Similarly, the catalytic activity needs to be further improved and special attention is needed to increase the catalytic role of SOFC composite anodes.

1.10 Anode catalyst- vanadium oxide

Vanadium pentoxide V_2O_5 is an active catalyst for oxidation of hydrocarbons and sulfur [66]. The double bond of vanadium and oxygen, $V=O$, is reactive and helps to efficiently oxidize the fuel making V_2O_5 a good anode catalyst [67]. In addition, when V_2O_5 is exposed to sour gas, its catalytic activity may reduce the carbon and sulfur deposition on the surface of the anode oxidizing these elements and preventing the poisoning of the catalyst. However, V_2O_5 is not stable and evaporates in high oxidizing environment above 750°C and its instability is more severe in presence of H_2S. In high reducing conditions, V_2O_5 may be reduced and form VO_2, V_2O_3, or VO depending on the severity of reduction, components with higher thermal but lower activity.

Recently, to increase the mechanical and thermal stability and activity of vanadium, this element is applied on the surface of different oxides such as SiO_2, Al_2O_3, ZrO_2, TiO_2 and CeO_2 [67, 68]. The higher oxidizing activity of supported vanadium, VO_x, is attributed to the interaction between the vanadium and the

27

support (M), V-O-M which makes the double bond of vanadium and oxygen, V=O, more reactive [69, 70]. Furthermore, by decreasing the thickness of the active layer, the mechanical strength, thermal stability increases.

There are many methods for depositing an active layer on the surface of the support, such as chemical vapor deposition and impregnation both are well known. Grafting is the recommendable method for getting a monolayer and a thin active layer made of well dispersed VO_x on the surface of the support [69, 70]. In grafting, the active phase is strongly bond on the surface of the support from adsorption of the precursor and subsequently hydrolysis reaction on the surface of the support. Finally the grafted particles are dried and calcinated to remove unreacted vanadium and hydroxyl groups.

During the synthesis, it is highly recommended to use a low concentration of precursor in order to graft a stable active phase on the surface of the support. High concentration of vanadium may lead to multiples layers with weak interaction and poor mechanical and thermal properties. The composition of the active phase on the surface of the support may vary depending on the preparation method, concentration of precursor, support and even pH. Studies have reported presence of V_2O_5, V_2O_3, VO_2, vanadate, poly vanadate on the surface of different supports [71]. All these possible compounds deposited on the surface make the studies of this catalyst and characterization very complex. Figure 1-6 shows different structures that vanadium oxide can possess on the surface of the support.
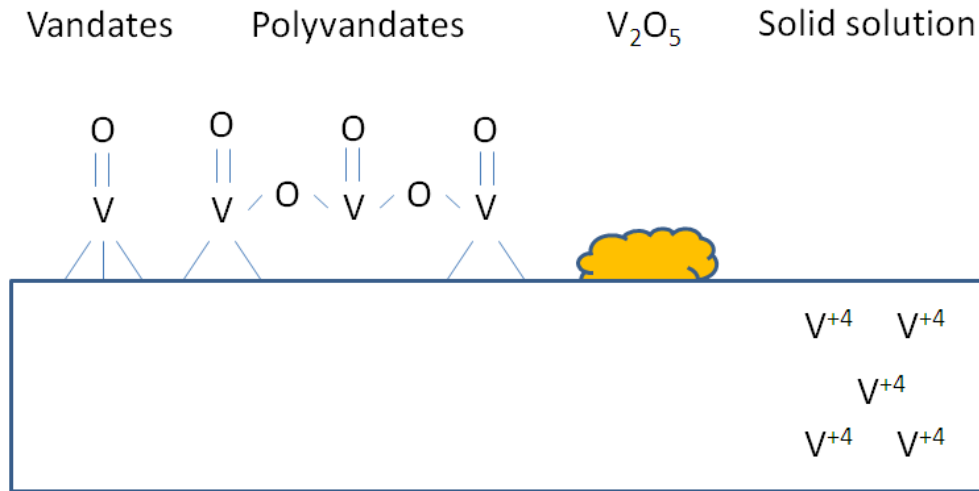
Figure 1-6 Structure of interface vanadium/support [71]

As mentioned, the interaction between the active layer and the support plays an important role in the stability and activity of the catalyst. The high affinity between vanadium and titanium species of their low electronegativity is very attractive and beneficial for metal oxide supported catalyst [69, 72]. Its affinity is even higher than the affinity exhibited by vanadium with silica. For example, 7 to 8 vanadium atoms are able to bond in 1 nm^2 of TiO_2 while 0.7 vanadium atoms are fairly bond in 1 nm^2 of SiO_2 [32].

$LSB_{10}T/YSZ$ is a composite anode with good stability in H_2S and relatively good electrochemical performance. Nevertheless, the catalytic role for oxidizing hydrocarbon has to be further improved. This composite suffer from carbon deposition on the surface and eventually degradation due its lack catalytic and oxidizing role. V_2O_5 has been proved to be a good hydrocarbon oxidizing but not stable enough in H_2S-containing gas at high temperature. On the other hand,

VO$_x$ grafted on TiO$_2$ has resulted to be more catalytic active than unsupported V$_2$O$_5$ and the strong interaction of the active phase, VO$_x$, and the support enhances the thermal and mechanical properties of the vanadium phase. VO$_x$/TiO$_2$ has been previously used to catalytically promote the oxidation various hydrocarbons but it has never been used for SOFC applications.

The objectives of this was to develop a catalyst to enhance the electrochemical performance, coking resistance and sulfur tolerance of SOFC fed with 5000 ppm of H$_2$S containing methane. For this purpose, VO$_x$ was grafted on the surface of TiO$_2$. The material and its catalytic activity were characterized. Then, the catalyst was introduced into a LSB$_{10}$T/YSZ porous composite anode, and the electrochemical performance, electrochemical stability, coking resistance and sulfur tolerance of SOFC were investigated.

References

[1] S. Shafiee, E. Topal, Appl.Energy, 87 (2010) 988-1000.

[2] World consumption of Primary Energy by Energy Type and Selected Country Groups, the Annual Energy Outlook 2008, U.S. Department of Energy, 2008.

[3] M.M. Gowen, Energy Policy, 17 (1989) 455-470.

[4] F. McGowan, Energy Policy, 19 (1991) 110-118.

[5] T.C. Coburn, B.C. Farhar, Public Reaction to Renewable Energy Sources and Systems, Encyclopedia of Energy, Elsevier, New York, 2004, pp. 207-222.

[6] L.G. Kemeny, Math.Comput.Simul., 24 (1982) 194-203.

[7] C.W. Garrett, Progress in Energy and Combustion Science, 18 (1992) 369-407.

[8] D.J. Wuebbles, A.K. Jain, Fuel Process Technol, 71 (2001) 99-119.

[9] S.G. Chalk, J.F. Miller, J.Power Sources, 159 (2006) 73-80.

[10] R.P. O'Hayre, Fuel cell fundamentals, 2nd ed., John Wiley & Sons, Hoboken, N.J.; 2009, pp. 546.

[11] P. Varbanov, J. Klemeš, Energy, 33 (2008) 1508-1517.

[12] A. Midilli, I. Dincer, Int J Hydrogen Energy, 33 (2008) 4209-4222.

[13] M.P. Hekkert, F.H.J.F. Hendriks, A.P.C. Faaij, M.L. Neelis, Energy Policy, 33 (2005) 579-594.

[14] S. Lim, J. Bae, K. Kim, Int J Hydrogen Energy, 34 (2009) 870-876.

[15] R.L. Keiski, O. Desponds, Y. Chang, G.A. Somorjai, Applied Catalysis A: General, 101 (1993) 317-338.

[16] S.K. Gangwal, Chapter 11 - Desulfurization for Fuel Cells, Elsevier, Amsterdam, 2011, pp. 317-360.

[17] L. Aguilar, S. Zha, Z. Cheng, J. Winnick, M. Liu, J.Power Sources, 135 (2004) 17-24.

[18] Fuel Cell Handbook, 6th Edition ed., EG&G Technical Services, Inc. Science Applications International Corporation, U.S. Department of Energy; 2002.

[19] Y. Wang, K.S. Chen, J. Mishler, S.C. Cho, X.C. Adroher, Appl.Energy, 88 (2011) 981-1007.

[20] G. Merle, M. Wessling, K. Nijmeijer, J.Membr.Sci., 377 (2011) 1-35.

[21] A.S. Martinez, J. Brouwer, Electrochim.Acta, 53 (2008) 3597-3609.

[22] J. Deseure, Y. Bultel, L. Dessemond, E. Siebert, Electrochim.Acta, 50 (2005) 2037-2046.

[23] B. Kenney, M. Valdmanis, C. Baker, J.G. Pharoah, K. Karan, J.Power Sources, 189 (2009) 1051-1059.

[24] M. Kleitz, F. Petitbon, Solid State Ionics, 92 (1996) 65-74.

[25] M. Andersson, J. Yuan, B. Sundén, Int.J.Heat Mass Transfer, 55 (2012) 773-788.

[26] M. Backhaus-Ricoult, Solid State Sciences, 10 (2008) 670-688.

[27] D.R. Crow, Principles and applications of electrochemistry, 4th ed., Blackie Academic & Professional, London ; New York, NY; 1994, pp. 282.

[28] A.V. Virkar, J. Chen, C.W. Tanner, J. Kim, Solid State Ionics, 131 (2000) 189-198.

[29] R.F. Mann, J.C. Amphlett, B.A. Peppley, C.P. Thurgood, J.Power Sources, 161 (2006) 775-781.

[30] F.S. Baumann, J. Maier, J. Fleig, Solid State Ionics, 179 (2008) 1198-1204.

[31] J. Fleig, J. Maier, Journal of the European Ceramic Society, 24 (2004) 1343-1347.

[32] A.V. Virkar, J. Chen, C.W. Tanner, J. Kim, Solid State Ionics, 131 (2000) 189-198.

[33] Y. Wang, K.S. Chen, J. Mishler, S.C. Cho, X.C. Adroher, Appl.Energy, 88 (2011) 981-1007.

[34] S.R. Choudhury, M.B. Deshmukh, R. Rengaswamy, J.Power Sources, 112 (2002) 137-152.

[35] E. Antolini, Appl.Energy, 88 (2011) 4274-4293.

[36] X. Zhang, S.H. Chan, G. Li, H.K. Ho, J. Li, Z. Feng, J.Power Sources, 195 (2010) 685-702.

[37] H. Wen, J.C. Ordonez, J.V.C. Vargas, Appl.Therm.Eng, 50 (2013) 12-25

[38] N. Yan, X. Fu, J. Luo, K.T. Chuang, A.R. Sanger, J.Power Sources, 198 (2012) 164-169.

[39] X. Fu, J. Melnik, Q. Low, J. Luo, K.T. Chuang, A.R. Sanger, Q. Yang, Int J Hydrogen Energy, 35 (2010) 11180-11187.

[40] Q. Low, W. Huang, X. Fu, J. Melnik, J. Luo, K.T. Chuang, A.R. Sanger, Appl.Surf.Sci., 258 (2011) 1014-1020.

[41] M. Backhaus-Ricoult, Solid State Sciences, 10 (2008) 670-688.

[42] J.C. Ruiz-Morales, J. Canales-Vázquez, D. Marrero-López, J.T.S. Irvine, P. Núñez, Electrochim.Acta, 52 (2007) 7217-7225.

[43] K. Park, S. Yu, J. Bae, H. Kim, Y. Ko, Int J Hydrogen Energy, 35 (2010) 8670-8677.

[44] K. Sasaki, K. Susuki, A. Iyoshi, M. Uchimura, N. Imamura, H. Kusaba, Y. Teraoka, H. Fuchino, K. Tsujimoto, Y. Uchida, N. Jingo, Journal of The Electrochemical Society, 153 (2006) A2023-A2029.

[45] A.R. Hanifi, A. Torabi, T.H. Etsell, L. Yamarte, P. Sarkar, Solid State Ionics, 192 (2011) 368-371.

[46] J. Rossmeisl, W.G. Bessler, Solid State Ionics, 178 (2008) 1694-1700.

[47] X. Zhai, S. Ding, Z. Liu, Y. Jin, Y. Cheng, Int J Hydrogen Energy, 36 (2011) 482-489.

[48] H. Koide, Y. Someya, T. Yoshida, T. Maruyama, Solid State Ionics, 132 (2000) 253-260.

[49] M. Gong, X. Liu, J. Trembly, C. Johnson, J.Power Sources, 168 (2007) 289-298.

[50] J.B. Wang, S. Hsiao, T. Huang, Applied Catalysis A: General, 246 (2003) 197-211.

[51] Y. Matsuzaki, I. Yasuda, Solid State Ionics, 132 (2000) 261-269.

[52] S. Zha, P. Tsang, Z. Cheng, M. Liu, Journal of Solid State Chemistry, 178 (2005) 1844-1850.

[53] P. He, M. Liu, J.L. Luo, A.R. Sanger, K.T. Chuang, Journal of The Electrochemical Society, 149 (2002) A808-A814.

[54] M. Liu, G. Wei, J. Luo, A.R. Sanger, K.T. Chuang, Journal of The Electrochemical Society, 150 (2003) A1025-A1029.

[55] H. He, R.J. Gorte, J.M. Vohs, Electrochemical and Solid-State Letters, 8 (2005) A279-A280.

[56] H. Inaba, H. Tagawa, Solid State Ionics, 83 (1996) 1-16.

[57] A. Tomita, K. Tsunekawa, T. Hibino, S. Teranishi, Y. Tachi, M. Sano, Solid State Ionics, 177 (2006) 2951-2956.

[58] Y. Huang, R.I. Dass, Z. Xing, J.B. Goodenough, Science, 312 (2006) 254-257.

[59] Z. Cheng, S. Zha, L. Aguilar, M. Liu, Solid State Ionics, 176 (2005) 1921-1928.

[60] S. Hui, A. Petric, Solid State Ionics, 143 (2001) 275-283.

[61] A. Marina, L.R. Pederson, Proceedings of the 5th European Solid Oxide Fuel Cell Forum, European SOFC Forum, Lucerne,Switzerland, (2002) 481.

[62] A. Vincent, J. Luo, K.T. Chuang, A.R. Sanger, J.Power Sources, 195 (2010) 769-774.

[63] J.T.S. Irvine, Perovskite Oxide Anodes for SOFCs, Springer US, 2009, pp. 167-182.

[64] D. Burnat, A. Heel, L. Holzer, D. Kata, J. Lis, T. Graule, J.Power Sources, 201 (2012) 26-36.

[65] J.W. Fergus, Solid State Ionics, 177 (2006) 1529-1541.

[66] I.E. Wachs, Catalysis Today, 100 (2005) 79-94.

[67] J.P. Dunn, H.G. Stenger Jr., I.E. Wachs, Catalysis Today, 51 (1999) 301-318.

[68] F. Arena, F. Frusteri, A. Parmaliana, Applied Catalysis A: General, 176 (1999) 189-199.

[69] G.C. Bond, Applied Catalysis A: General, 157 (1997) 91-103.

[70] E. Santacesaria, M. Cozzolino, M. Di Serio, A.M. Venezia, R. Tesser, Applied Catalysis A: General, 270 (2004) 177-192.

[71] J. Haber, Catalysis Today, 142 (2009) 100-113.

[72] G.C. Bond, S.F. Tahir, Applied Catalysis, 71 (1991) 1-31.

Chapter 2   Electrical and electronic conductivity measurements of Ba doped LST

2.1 Introduction

A composite anode should possess a set of properties to exhibit good performance in SOFCs using sulfur-containing hydrocarbon fuels, for example, catalytic activity, thermal and mechanical stability, sulfur and carbon tolerance, and electrical conductivity. Special attention should be addressed on the electrical conductivity to overcome resistance polarization, the main source of voltage drop in SOFCs. For this reason, perovskite has been extensively investigated due its mixed electronic and ionic conductivity, stability and activity, making this material suitable for SOFC applications.

Strontium titanate, $SrTiO_3$, is a perovskite with an n- type electronic conductivity at low partial pressure of oxygen. To further increase its conductivity, new element with different valences and oxidation states are doped at the A site of the perovskite, such as, Ba doped $SrTiO_3$ [1], Y doped $SrTiO_3$ [2] and La doped $SrTiO_3$ [3, 4]. Provided to its high stability in H_2S environments, LST has become an attractive material for SOFC applications.

On top of having good sulfur tolerance, LST is also known for the high electrical conductivity. The high conductivity is achieved when $SrTiO_3$ is doped with La at the A site of the perovskite to increase the ionic and electrical conductivity of this compound. La acts as donor to increase the oxygen vacancies of the $SrTiO_3$ and partly reduce Ti^{4+} to Ti^{3+}. At this point, electrons easily

introduce to the T-3d orbital [4] and force the compound to behave as n-type conductor. The further electron hopping re-oxidizes Ti $^{3+}$ to Ti^{4+}.

When LST is exposed to low partial pressure of oxygen, Ti $^{4+}$ is reduced to Ti^{3+} introducing more oxygen vacancies and increasing the electronic conductivity. For this reason, when LST is sintered under reducing conditions, the electronic and electrical conductivity may increase substantially. In contrast, when LST is sintered under oxidizing conditions, titanium is likely to exhibit a valence Ti^{4+} and the oxygen content build up to the keep electro neutrality in the structure.

Independent of the sintering conditions, LST usually exhibits high electronic conductivity with low ionic conductivity. For SOFC anodes, it is fundamental to have high electrical conductivity with commensurable electronic and ionic conductivity to transport oxide ions and electrons, and carry out all the electrochemical reactions. Consequently, efforts have been made to dope the B-site of the LST and increase the ionic conductivity. By doping the B-site with cations of different valences, the introduction of new oxygen vacancies promotes higher ionic conductivity. For example, it has been reported than doping LST with cobalt, at the B-site, the ionic conductivity increases [5].

Our research group has proposed LSB$_{10}$T where a small fraction of the strontium is substituted for barium to increase the catalytic activity of the LST. In addition the presence of barium, an element with a larger size than strontium, at the B-site increases the free volume of the structure and may promote higher

mobility of the carries and electrical conductivity [6]. This new perovskite has resulted in higher electrochemical performance than that of LST and good sulfur tolerance [7]. However, the electronic and ionic conductivities and influence of the sintering atmosphere on these properties have not been reported yet.

The high ionic conductivity of YSZ, lack of reactivity and similar TEC with other perovskite make possible to make mixtures of YSZ and other perovskite as a composite anode. For example, most of the time,   LST is mixed with YSZ to increase the power density and energy conversion of the SOFCs.

Regarding the characterization, there are some studies specialized on measuring the total conductivity of MIEC, but just few of them are focused on discerning the specific contribution of the ionic and electronic conductivities to the total conductivity. Studying the electronic and ionic conductivity allows better understanding of the conductivity mechanisms in ceramics and optimization tool.

The electromotive force method, EMF, Faradic Efficiency cell and blocking electrodes, BE, are the most used characterization methods to discern the ionic and electronic conductivities. EMF is a driving force developed in a concentration cell. In these conditions, it is possible to calculate the oxide ionic and electronic transport number using the theoretical equilibrium potential and the experimental open circuit voltage of the cell registered in the experiment. The electronic and ionic transport number indicates the contribution of the electronic and ionic conductivity to the electrical conductivity respectively [8]. This method is very convenient for its simplicity in measurements with cells subjected to

different partial pressures [9-11]. Nevertheless, a multiple ion conductor makes the conductivity measurement very complex [12].

The faradic efficiency cell is another method to quantify the ionic conductivity of a MIEC. In this method, the current that is necessary to polarize a symmetrical cell and change the partial pressure of oxygen in one side of the chamber is calculated [10]. Consequently, to keep the same conditions in each side, zirconia sensors are used to add oxygen and compensate the change in pressure. The concentration of oxygen added to the system is proportional to the concentration of oxide ions transported through the ionic conductor.

BE consists in measuring either the ionic or electronic current of a MIEC that passes through an electronic or ionic blocking electrode [13]. The experiment is simple but there some recommendation to follow. First, the resistance of the blocking electrode should be less than the resistivity of the MIEC. Otherwise, the registered property will be more likely related to the conductivity of the blocking electrode. Second, polarization at the reversible electrodes should be low to avoid under estimation of the conductivity of the MIEC. Platinum can be use used as reversible electrode since it is relatively inert. Regarding contact resistances, one effective way to reduce it, is by using four probe measurements in thick samples, for example, Van der Paw [13]. Demircan et al. measured the resistivity of Ni/YSZ composite SOFC anodes using Van der Paw [14]. According to Etsell et al. [15], two probe measurements can yield accurate values at relatively low temperatures, T <1400° C. Finally, the blocking electrode has to be very dense to avoid diffusion of the gas as well as it has to be thinner than the MIEC.

BE can be used in a symmetrical or concentration cell. For example, Hebb-Wagner polarization method with BE is a concentration cell that uses different partial pressures of oxygen to measure the oxide ionic conductivity of the sample. It is a suitable experiment to identify type of conductivity of the MIEC, p-type or n-type, at different temperatures [16-18].

This study is based on the measurements of the ionic and electronic conductivities of YSZ, $LSB_{10}T$ and $LSB_{10}T$ impregnated YSZ samples using BE method.

2.2 Experimental procedure

2.2.1 Synthesis of $LSB_{10}T$

$LSB_{10}T$, was prepared using solid state synthesis. Proper ratios of La_2O_3 (Alfa Aesar 99.99%), TiO_2 (mixed anatase and rutile 99.5%, <100 nm, Aldrich), $SrCO_3$ (Alfa Aesar 99 %) and $BaCO_3$ (Fisher 99.4%) were mixed, grinded, pressed and calcinated in air at 1200°C for 4 hours. The resulting powder was further milled with zirconia balls for 6 hours, pressed uniaxial at 179 MPa and sintered in forming gas (5% H_2-N_2) at 1400 °C for 5 hours to prepare pellets with 2 mm thick. Finally, dense YSZ pellets with, 1 mm thick and apparent density of 5.95 gr/cm^3 were prepared by pressing uniaxially YSZ powder (Tosho) at 179 M Pa and sintered for 5 hours at 1500°C in air.

To measure the electrical conductivity of $LSB_{10}T$ impregnated porous

YSZ, YSZ disks with 40 % porosity and 1 mm thick were prepared by intimately mixing YSZ powder (Tosho) with pore former precursor, polymethylmethacrylate, PMMA, and pressing uniaxially the resulting YSZ/PMMA mixture at 179 M Pa and sintered for 5 hours at 1500°C in air..

A LSB$_{10}$T solution was prepared by mixing proper ratios, lanthanum nitrate, La(NO$_3$)$_3$.6H$_2$O (Alfa Aesar 99.9%), strontium nitrate, Sr(NO$_3$)$_2$ (Sigma Aldrich), and barium nitrate, Ba(NO$_3$)$_2$ (Alfa Aesar 99%) solubilized in ultra-pure water and Triton X100 with a solution containing titanium isopropoxide, citric acid and hydrogen. Then, the LSB$_{10}$T solution was slowly mixed under vigorous stirring and vacuum assisted infiltrated inside the porous YSZ. Finally the impregnated samples were calcinated at 800°C for 4 hours to get a final concentration of 12 wt. % of LSB$_{10}$T inside the porous YSZ matrix.

2.2.2 Characterization of material properties

Images of sintered YSZ, LSB$_{10}$T and LSB$_{10}$T impregnated YSZ samples were examined using a scanning electron microscope (Hitachi S-2700).

The electrical conductivity of YSZ, LSB$_{10}$T, and LSB$_{10}$T impregnated porous YSZ samples were measured using DC polarization in a commercial NorECs Probostat electrochemical cell with platinum and gold current collectors (two probes configuration) and Equation 2-1:

$$\sigma = t * (A * R_{measured})^{-1} \qquad\qquad \textbf{2-1}$$

where t is the thickness of the sample, R is the resistance of the sample and A the area of the sample.

The electrochemical cell consisted in a concentration cell supplied in one compartment with 10% $O_2 - N_2$, and the other compartment with 10% $H_2 - N_2$, both flowing at 50 mL/min. In addition, Van der Paw (four probe configuration) was set up on a thick YSZ disk exposed in 10% $O_2 - N_2$ flowing at 50 mL/min to determine the effect of contact resistance on the measurement.

The ionic and electronic conductivities of the samples were measured with BE using the concentration cell. For YSZ samples, the electronic conductivity was measured using gold foil as the BE and 1 cm^2 platinum ink was painted in both sides as the reversible electrode. Au paste was printed between the YSZ sample and the BE to minimize the contact resistance at the interface.

Ionic conductivities of $LSB_{10}T$ and $LSB_{10}T$ impregnated porous YSZ samples were measured using a thin and dense YSZ layer as the BE. 1 cm^2 platinum paste was printed on both side of the sample as reversible electrode and at the interface of the sample and BE to reduce contact resistance. All samples were tested at each temperature, 700°C, 750°C, 800°C, 850°C and 900°C.

Figure 2-1 shows the schematic diagrams for measuring electronic and ionic conductivities:
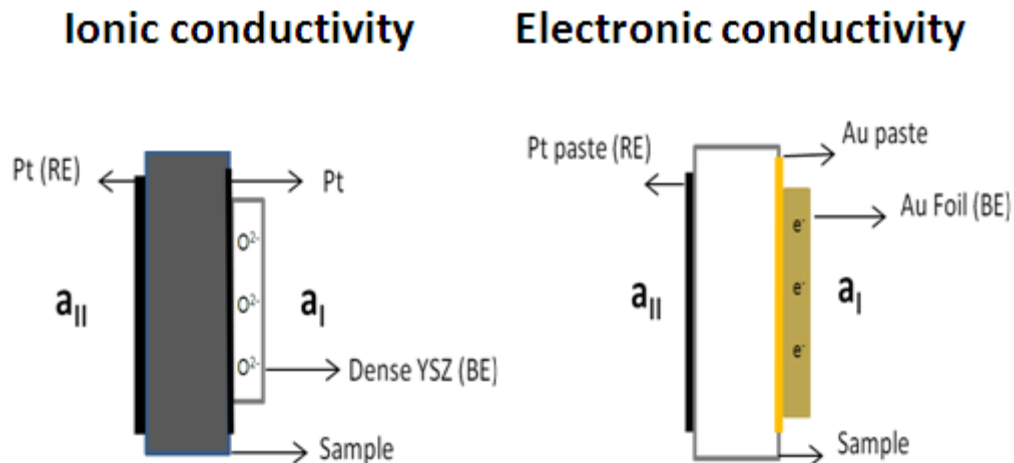
Ionic conductivity

Electronic conductivity

Figure 2-1 Electronic and Ionic measurements with BEs

2.3 Results and discussions

2.3.1 YSZ conductivity studies

In order to confirm the accuracy and confident level of the proposed set up with BE, the electrical and ionic conductivity of YSZ, a material which had been extensively studied,   was measured.

YSZ pellet cross section is shown in Figure 2-2. The pellet exhibited intimate contact of the particles and very low porosity after being sintered in air for 5 hours. The total conductivity of YSZ samples were measured in a two-probe concentration cell and four-probe symmetrical cell, Van der Paw, from 700°C to 900°C.
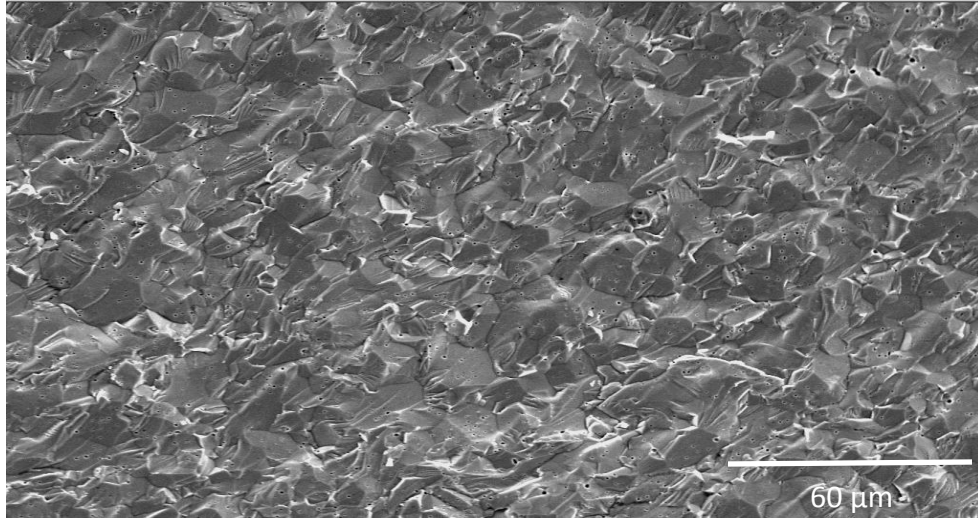
60 µm

Figure 2-2 Cross section of the YSZ sample

Figure 2-3 shows the total conductivities of the YSZ as a function of temperature using two- and four-probe conductivity measurements. It is noticeable the direct dependency of the conductivity on the temperature, and the low contact resistance based on the similar conductivities using two- and four-probe conductivity measurements. Moreover, it is evident that despite of the different partial pressure of hydrogen at which YSZ samples were subjected, this pressure doesn't have influence on the ionic conductivity of the samples, confirming the pure oxide ion conductivity properties of YSZ.
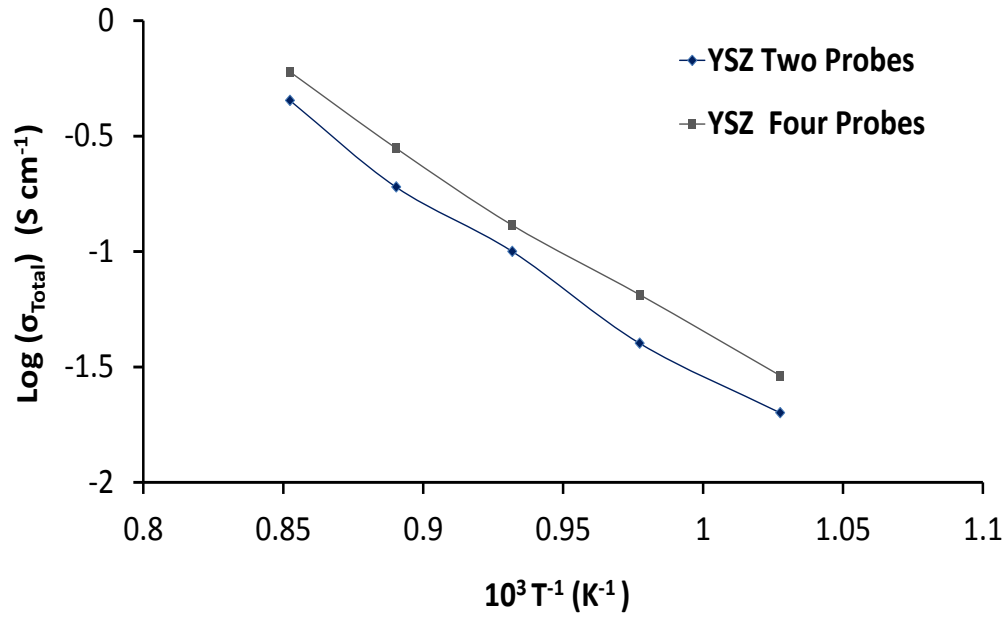
Figure 2-3 Total conductivity of the YSZ sample

The electronic conductivity of YSZ was measured with the two probes concentration cell using gold foil as BE. As shown in Figure 2-4, the electronic conductivity increases with an increase in the temperature. The contribution of this electronic conductivity to the total conductivity is small, almost negligible. At 700°C the electronic conductivity YSZ is 0.0008 $\Omega^{-1}cm^{-1}$, this is only 4% of the total conductivity.
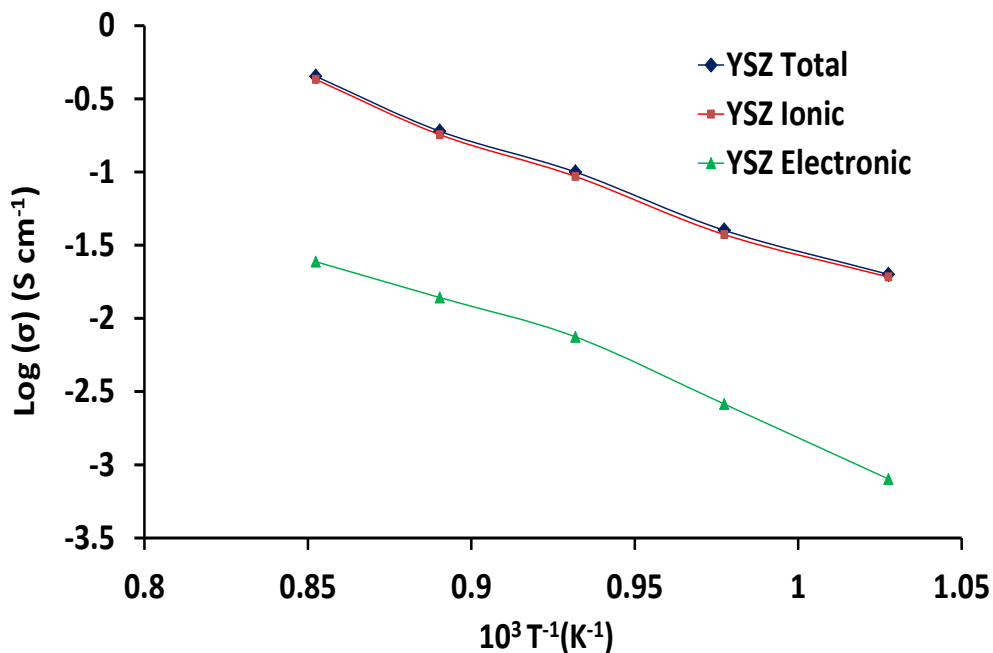
Figure 2-4 Electronic, ionic and total conductivity of the YSZ sample

The ionic and electronic transport numbers were deduced from the experimental data. Table 2-1 shows the ionic transport number using BEs and electro motive force, EMF. The measured transport numbers at all temperatures are close with both methods, validating the accuracy of experiments with BE. The lowest ionic transport number was 0.95, providing the evidence of the high ionic conductivity of YSZ. Such high ionic conductivity avoids the drop of the OCV or equilibrium voltage. For this reason, YSZ is widely used as electrolyte for solid oxide fuel cell applications.

	EMF	B E
700°C	0.97	0.96
750°C	0.98	0.94
800°C	0.97	0.94
850°C	0.96	0.95
900°C	0.96	0.95

Table 2-1 Ionic transport number of YSZ

2.3.2 LSB$_{10}$T conductivity studies

LSB$_{10}$T pellets, previously sintered in forming gas and air, where prepared to study the effect of the sintering conditions on the conductivity of the perovskite. The cross section of the pellet is shown in Figure 2-5. The sample possesses a high density and relatively uniform particle size.
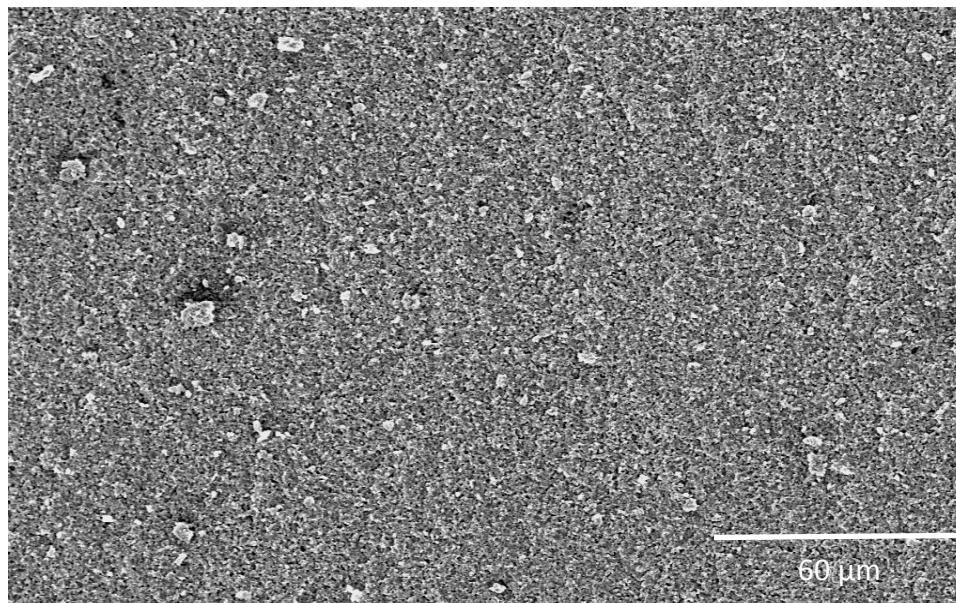

Figure 2-5 Cross section of LSB$_{10}$T samples

The reduced $LSB_{10}T$ and oxidized $LSB_{10}T$ exhibited higher electrical conductivity than YSZ, having an exponential dependence on the temperature, as shown in Figure 2-6. The reduced $LSB_{10}T$ has higher total conductivity than the oxidized $LSB_{10}T$ at all temperatures. At 700°C, the reduced $LSB_{10}T$ registers 3 $\Omega^{-1}cm^{-1}$ while the oxidized registers of 0.4 $\Omega^{-1}cm^{-1}$, a conductivity gap of one order difference. On the other hand, at higher temperature this gap is less evident, at 900°C the reduced $LSB_{10}T$ registers 7.5 $\Omega^{-1}cm^{-1}$ while the oxidized $LSB_{10}T$ registers 4.5 $\Omega^{-1}cm^{-1}$. These differences are attributed to the sintering conditions and concentration of oxygen vacancies created during the sintering of the $LSB_{10}T$ in reducing and oxidizing conditions.

When the oxidized $LSB_{10}T$ is tested in the concentration cell, it is partially reduced creating oxygen vacancies and increasing the total conductivity. The partial reduction increases at higher temperatures, promoting higher electrical conductivity. This behavior highlights the important role of the partial pressure of hydrogen in the introduction of oxygen vacancies and conductivity of this perovskite.
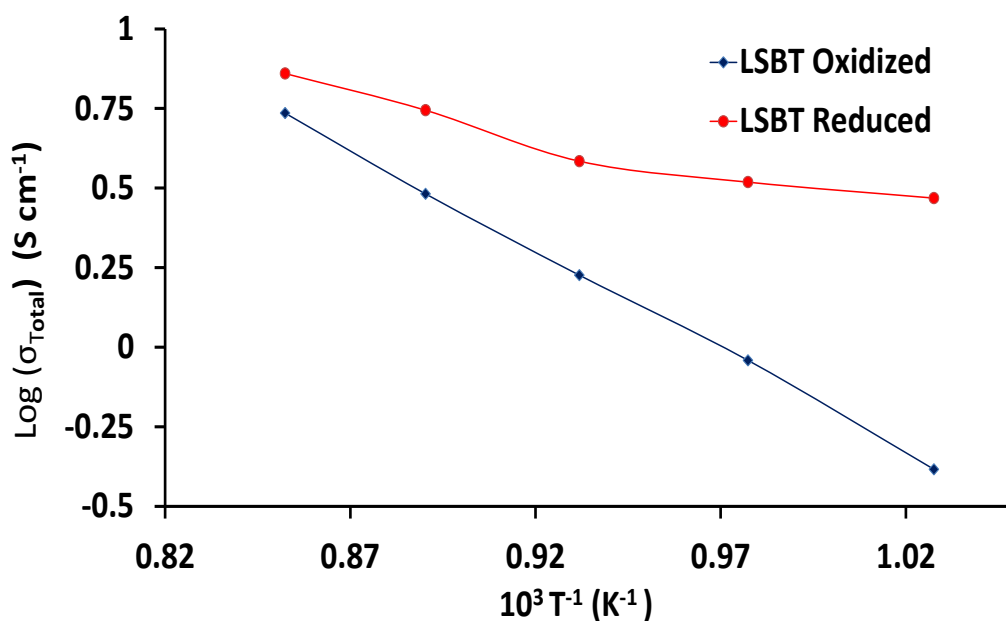
Figure 2-6 Total conductivity of LSB$_{10}$T samples

For a better understanding of the effect of the sintering condition on the conductivity, the ionic conductivity of the samples was discriminated, as shown in Figure 2-7. The oxidized LSB$_{10}$T exhibits higher ionic conductivity than the reduced LSB$_{10}$T from 700°C to 900°C. In fact, when LSB$_{10}$T is initially sintered in air, the LSB$_{10}$T is oxidized by a fraction, δ, from La$_{0.4}$Sr$_{0.5}$Ba$_{0.1}$TiO$_3$ to La$_{0.4}$Sr$_{0.5}$Ba$_{0.1}$TiO$_{3+δ}$, producing an excess of oxygen that might be stored inside. By adding barium and partially substituting strontium, the lattice parameter of the perovskite increases following the Vegard's law [7], allowing more oxygen storage at either random or interstitial places and increasing the amount of oxygen vacancies and mobility when the oxidized sample is further exposed at reducing conditions.
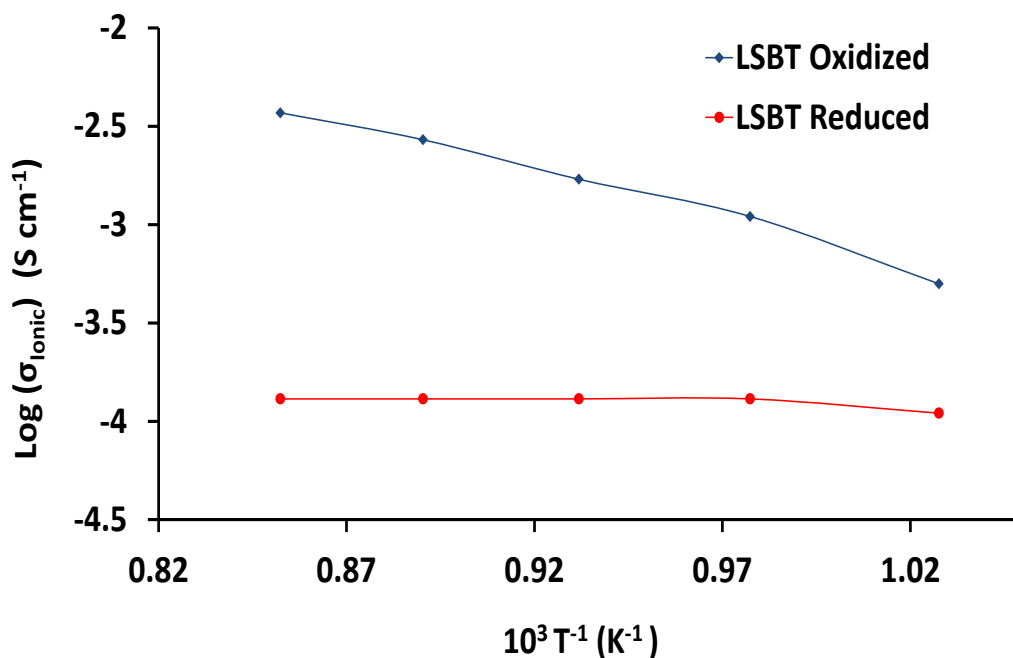
48

Figure 2-7 Ionic conductivity of LSB$_{10}$T samples

The electronic conductivities of the samples were calculated by subtracting the ionic conductivity from the total conductivity and the results are shown in Figure 2-8. At oxidizing sintering conditions, Ti is forced to be tetravalent, 4+, rather than trivalent, 3+, this last form is thought to be responsible for the high electronic conductive of the perovskite. For this reason, initially the oxidized LSB$_{10}$T has lower electronic conductivity than the reduced LSB$_{10}$T. When the oxidized LSB$_{10}$T is exposed to reducing condition and higher temperatures, the removal of oxygen promotes oxygen vacancies and free electrons which are conducted by trivalent titanium, allowing the hopping of the free electrons along the structure enhancing the electronic and electrical conductivity.

Equation 2-2 describes the conductivity mechanism of the $LSB_{10}T$, the production of free electrons and oxygen vacancies from oxygen at substitutional point defects of the Perovskite.

$$\frac{1}{2}O_2 + V_o^{\cdot\cdot} + 2e^- \rightarrow O_o^x \qquad\qquad \textbf{2-2}$$
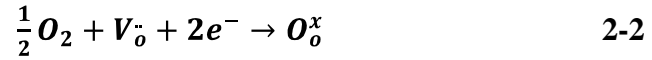
If $LSB_{10}T$ is sintered at high reducing condition, it is reduced by a fraction $-\delta$, from $La_{0.4}Sr_{0.5}Ba_{0.1}TiO_3$ to $La_{0.4}Sr_{0.5}Ba_{0.1}TiO_{3-\delta}$ and introducing some oxygen vacancies. These vacancies might increase the ionic conductivity but the severity of the reducing condition produces a rich trivalent titanium compound able to faster transport free electrons which are produced during the creation of oxygen vacancies. As a result, the perovskite exhibits a predominant n-type and high electronic conductivity. In contrast, the concentration of oxygen vacancies of the reduced $LSB_{10}T$ is not high enough to either increase the concentration of oxide ions and ionic conductivity.
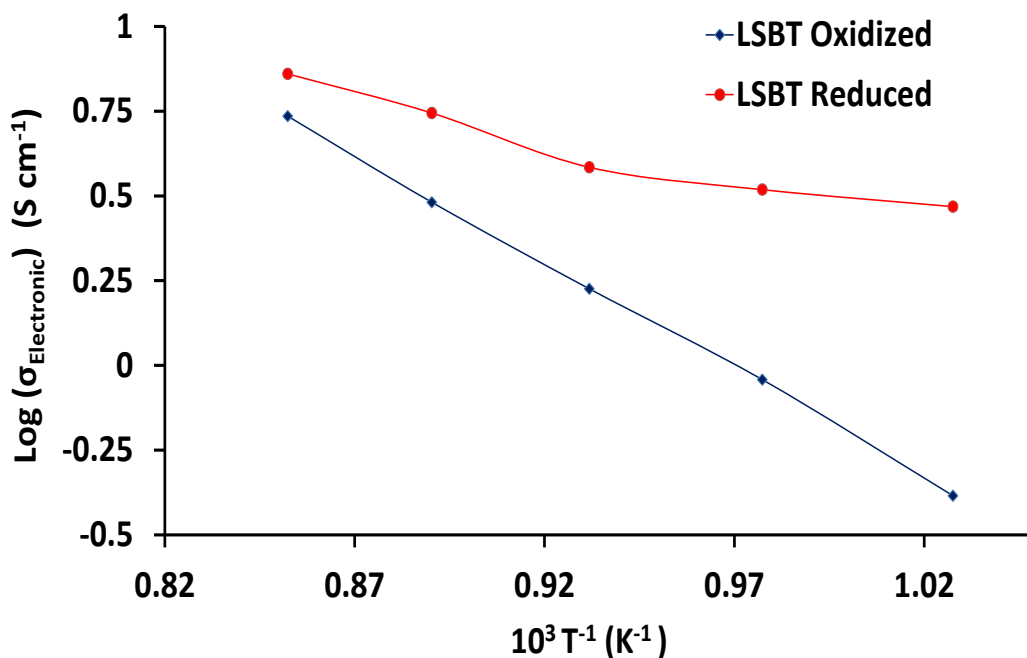
Figure 2-8 Electronic conductivity of LSB$_{10}$T

Table 2-2 compiles the calculated electronic transport number with EMF and BE for different samples. According to these values, the oxidized LSB$_{10}$T has higher ionic conductivity than the reduced LSB$_{10}$T, yet this type of conductivity is negligible compare to the electronic conductivity. Furthermore, independent of the sintering condition, none of the electronic transport numbers were less than 0.99, confirming the predominant electronic conductivity of the perovskite. In fact, the low oxide ion conductivity decreases the OCV, ionic transport number and head to short circuit with the EMF method.

51

	Oxidized		Reduced	
	EMF	BE	EMF	BE
700°C	0.990	0.990	0.999	0.997
750°C	0.990	0.990	0.999	0.997
800°C	0.990	0.980	0.999	0.997
850°C	0.990	0.980	0.999	0.997
900°C	0.990	0.980	0.999	0.997

Table 2-2 Electronic transport number of LSB$_{10}$T

2.3.3 LSB$_{10}$T impregnated YSZ conductivity studies

Porous YSZ samples were impregnated with LSB$_{10}$T in attempt to improve the microstructure of the composite material and conductivity. After infiltrating 12 wt. % of LSB$_{10}$T inside the porous YSZ, the efficiency of the infiltration decreased dramatically and higher amount was unachievable.

The ionic and electronic conductivities of the porous samples were measured with BE. The relationship between the conductivity of a dense sample, **σ**, the conductivity of a porous sample, **σ$_{porous}$**, and volume fraction porosity, **v_v**, is given by equation 2-3 [19, 20].   Figure 2-9 shows the registered electronic and ionic conductivity of the impregnated samples. It is evident that both conductivities increase with an increase in temperature due to faster mobility of the charge carriers, oxide ions and electrons, thorough the composite anode.
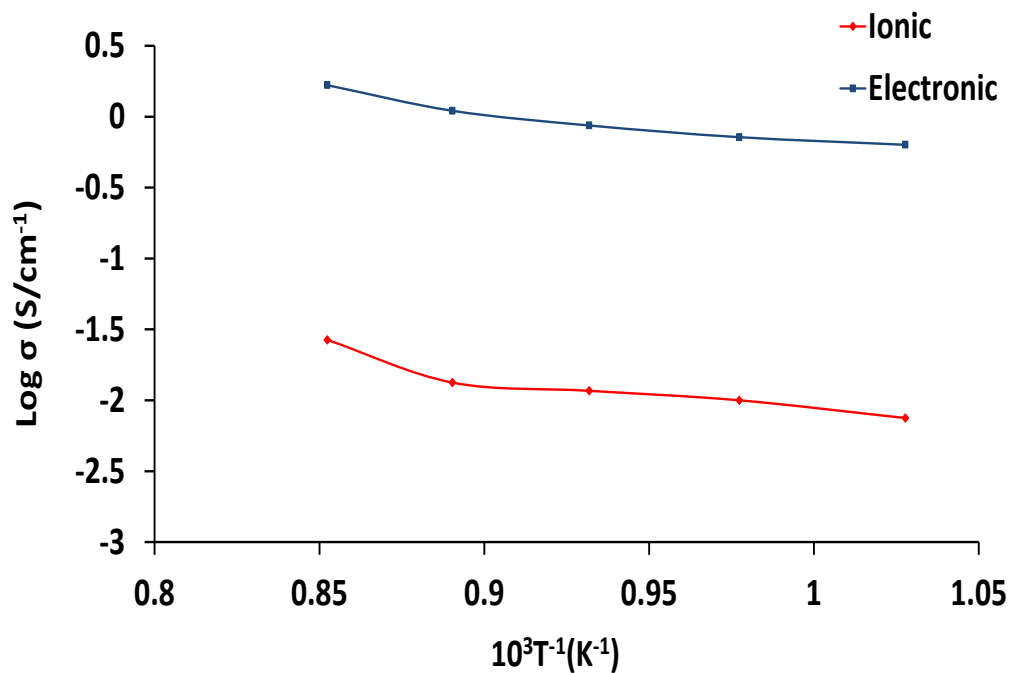
$$\sigma = \sigma_{porous} * (1 - v_v)^{-1} \qquad\qquad \textbf{2-3}$$

Figure 2-9 Ionic and Electronic conductivity of $LSB_{10}T$ impregnated YSZ sample

One might expect that the ionic conductivity of the $LSB_{10}T$ impregnated sample would be mainly conferred by the properties of YSZ. However, according to Figure 2-9, the sample exhibited lower ionic conductivity than the conductivity measured in the pure YSZ, as shown in Figure 2-4, but higher than those registered in pure $LSB_{10}T$, as shown in Figure 2-7, at the same temperature range and conditions. Then, it seems that most of the ionic conductivity of this composite is rather conferred by the properties of the $LSB_{10}T$, and the YSZ matrix just helped to increase this type of conductivity by small fraction.

On the other hand, the electronic conductivity of $LSB_{10}T$ impregnated sample is similar to the conductivity of the oxidized $LSB_{10}T$ and slightly lower

than the reduced $LSB_{10}T$ at the experimental temperature range, as shown in Figures 2-9, 2.8, and 2-10. This result is reasonable since the $LSB_{10}T$ impregnated porous YSZ was not sintered or severe thermal treated in reducing conditions. This measured electronic conductivity confirms that the conductivity of the impregnated sample comes from the properties of the $LSB_{10}T$.

In order to elucidate this behavior, the morphology of the cross section of the impregnated sample was analyzed and the SEM image is shown in Figure 2-10. $LSB_{10}T$ particles of around 60 nm were deposited on the surface of YSZ. These particles are agglomerated forming an electronic conductive layer that may partially block the normal flow of the oxide ions coming from the YSZ, decreasing the overall oxide ion conductivity of the impregnated sample, and making the electronic conductivity the main conductivity.
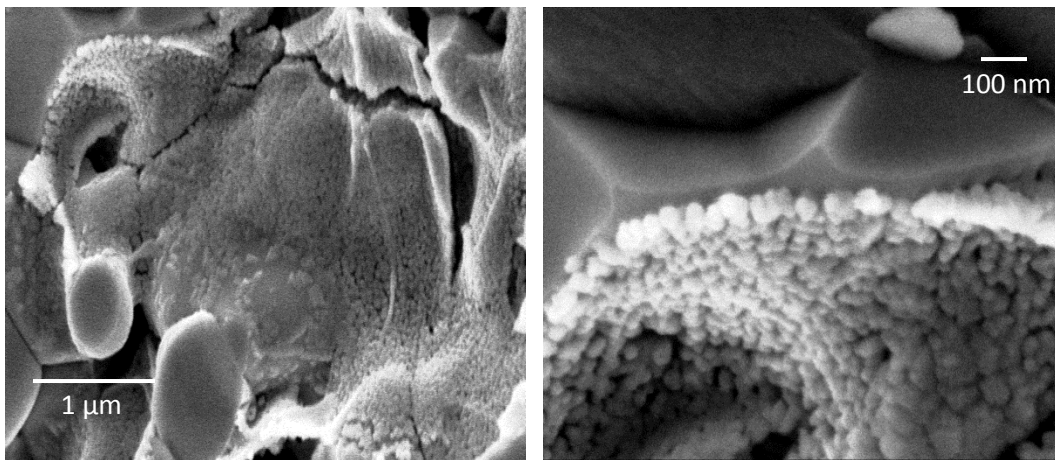

Figure 2-10 $LSB_{10}T$ impregnated YSZ sample

2.4 Conclusion

Conductivities of YSZ and LSB$_{10}$T were measured successfully with a two -probe concentration cell. YSZ exhibited high ionic conductivity while the LSB$_{10}$T exhibited a predominant electronic conductivity. The high electronic conductivity of the perovskite resides on the presence of the reduced form of Ti, Ti^{3+}, which acts as carrier of free electrons. The higher concentration of Ti^{3+} achieved when the sample is previously ex-situ sintered at reducing condition increases the electronic and total conductivity. Nonetheless, the ionic conductivity is small.

Under the oxidizing sintering condition, the addition of barium increases the lattice parameter of the perovskite and free volume and plays an important role in the oxygen storage, producing more oxygen vacancies and higher mobility of the carriers when the sample is re-exposed to reducing conditions. Despite of the increasing ionic conductivity, this is still negligible compare to the electronic conductivity. Finally, the electronic transport number measured with BE and EMF also highlights the high electronic conductivity of the perovskite, 0.99 in all the samples.

When LSB$_{10}$T is impregnated inside of a porous YSZ, the conductivity is predominantly electronic. The presence of YSZ helps to increase the ionic conductivity of the sample by a small portion. A continuous layer made of agglomerated LSB10T particles is formed on the surface of the YSZ, partially

blocking the migration of oxide ions and conducting electrons only. As a consequence, the LSB$_{10}$T impregnated YSZ exhibits a predominant electronic conductivity.

References

[1] J. Li, X. Fu, J. Luo, K.T. Chuang, A.R. Sanger, J.Power Sources, 213 (2012) 69-77.

[2] P. Puengjinda, H. Muroyama, T. Matsui, K. Eguchi, J.Power Sources, 204 (2012) 67-73.

[3] C.D. Savaniu, J.T.S. Irvine, Solid State Ionics, 192 (2011) 491-493.

[4] D. Burnat, A. Heel, L. Holzer, D. Kata, J. Lis, T. Graule, J.Power Sources, 201 (2012) 26-36.

[5] J.T.S. Irvine (Ed), Perovskite Oxide Anodes for SOFCs, Springer US, 2009, pp. 167-182.

[6] X. Li, H. Zhao, N. Xu, X. Zhou, C. Zhang, N. Chen, Int J Hydrogen Energy, 34 (2009) 6407-6414.

[7] A. Vincent, J. Luo, K.T. Chuang, A.R. Sanger, J.Power Sources, 195 (2010) 769-774.

[8] D.R. Crow, Principles and applications of electrochemistry, 4th ed., Blackie Academic & Professional, London ; New York, NY; 1994, pp. 282.

[9] S. Wang, L. Wu, J. Gao, Q. He, M. Liu, J.Power Sources, 185 (2008) 917-921.

[10] V.V. Kharton, A.A. Yaremchenko, A.P. Viskup, G.C. Mather, E.N. Naumovich, F.M.B. Marques, Solid State Ionics, 128 (2000) 79-90.

[11] H.K. Bentzer, N. Bonanos, J.W. Phair, Solid State Ionics, 181 (2010) 249-255.

[12] T. Norby, Solid State Ionics, 28–30, Part 2 (1988) 1586-1591.

[13] I. Riess, D.S. Tannhauser, Solid State Ionics, 7 (1982) 307-315.

[14] O. Demircan, C. Xu, J. Zondlo, H.O. Finklea, J.Power Sources, 194 (2009) 214-219.

[15] T. Etsell , S. Flengas, Chemical Reviews, 70 (1970) 3.

[16] T. Shimonosono, Y. Hirata, Y. Ehira, S. Sameshima, T. Horita, H. Yokokawa, Solid State Ionics, 174 (2004) 27-33.

[17] J.H. Jang, G.M. Choi, Solid State Ionics, 154–155 (2002) 481-486.

[18] S. Lübke, H.-. Wiemhöfer, Solid State Ionics, 117 (1999) 229-243.

[19] F. Zhao, A.V. Virkar, J.Power Sources, 195 (2010) 6268-6279.

[20] J. Wright, A.V. Virkar, J.Power Sources, 196 (2011) 6118-6124.

Chapter 3 VO$_x$/TiO$_2$ anode catalyst for oxidation of CH$_4$ containing 5000 ppm H$_2$S for SOFC

3.1 Introduction

The perovskite has received great attention as this structure possesses mixed ionic and electronic conductivity and for their suitability in SOFC applications. Furthermore, some perovskite structures have shown relatively good sulfur tolerance and conductivity enhancement when they were modified [1]. For example LSC shows stability in H$_2$S and good activity for oxidation reactions but the conductivity is low and need to be further improved. LSC might be doped with manganese to increase the conductivity but at the expense of lower sulfur tolerance [2]. Similarly, LSV has good conductivity and sulfur poisoning resistance but it is not redox stable enough. When LSV is oxidized, it rather acts as insulator than a conductor compound [3].

LST is another type of perovskite with prominent electronic conductivity and good stability at low and high concentration of H$_2$S [4]. The lack of activity limits its application in fuel cell fueled with hydrocarbons. Ba doped LST shows better activity for oxidation of hydrocarbons keeping the sulfur tolerance and electronic conductivity [5]. Due to the predominant electronic conductivity in these perovskite, they are usually mixed with YSZ, a pure oxide ion conductor and sulfur tolerant compound, for SOFC composite anode applications. In addition, in attempt to further improve the activity of the composite anode, this

component can be mixed with a third element, usually a catalyst that helps to enhance the selective oxidation of hydrocarbon and reduce carbon deposition.

In this order, vanadium pentoxide, V_2O_5, seemed to be a viable catalyst to enhance the oxidation of hydrocarbons and sulfur in SOFCs [6]. The vanadium-oxygen bonds are labile toward oxidation of different feed components and make V_2O_5 very active. Furthermore, when the catalyst is exposed to sour gas, its oxidization activity may also serve to reduce the amounts of carbon and sulfur deposited on the surface by promoting their oxidation to the corresponding oxides, thereby reducing propensity to poisoning of the catalyst. However, some properties of this compound impose drawbacks on its application in SOFC. First, the operating temperatures of SOFC typically are high, 700-1000°C, and, as the melting point of the V_2O_5 is below this range, 690°C, the catalyst will be subject to physical changes. Secondly, when it is exposed to high concentration of H_2S, the vanadium is sulfurized, which further reduces its melting point. However, when the V_2O_5 is in reducing environment, it may be reduced to one or more of VO_2, V_2O_3 and VO, depending on the severity of reduction. These products have higher melting points than V_2O_5, increasing the catalyst's physical stability at the operating temperatures of the SOFC, but their activity for oxidation reactions is less than that of the parent oxide.

Currently, vanadium oxide based catalysts often are supported on different oxides such as SiO_2, Al_2O_3, ZrO_2, TiO_2 and CeO_2 [7, 8], and by so supporting the vanadium oxide its catalytic activity can be increased by the interaction of the active phase and the support [8]. The higher oxidizing activity of supported

59

vanadium oxide catalysts, VO_x/support, is attributed to vanadium-oxygen-support bonds, since these bonds make more reactive the oxygen of the vanadium-oxygen double bonds [9, 10]. Furthermore, by having a thin and well dispersed active phase on the support, the mechanical strength and thermal stability increase and so grafting, absorption of the active element from a solution, is considered the best method to get a monolayer and a well dispersed VO_x, active phase on the surface of the support [8].

In contrast to other processes, in the grafting the precursors of the active layer are bound onto the surface of the support, a process that can involve adsorption of the precursor and hydrolysis reactions of the hydroxyl groups of the support. Typically, this is followed by calcination of the supported vanadium to remove unreacted vanadium precursors and the majority of the unreacted hydroxyl groups from the surface of the support. In addition, depending on the concentration of vanadium precursors, the available hydroxyl groups binding onto the support and the calcination process, the composition of the vanadium surface species may vary. One or more of V_2O_5, V_2O_3, VO_2, vanadate and polyvanadate moieties may be formed on the surface of the support, making studies of these metal oxides more complex [10].

As mentioned above, the interaction between the elements of the active layer and the support plays an important role in the stability and activity of the catalyst. The affinity of vanadium to titanium oxide support is higher than that with other supports such as silica, and this affinity is related to the relative electro negativities of the metals, where oxides of elements with lower electronegativity

than vanadium form stronger interactions with supported vanadium oxides. Beside, some studies also reveal that when vanadium is supported on titanium oxide, VO_x/TiO_2, it exhibits more activity for oxidation of hydrocarbons that the same catalyst bonded onto other supports [8, 10].

Hydrocarbon fuelled SOFC anodes suffer from carbon deposition and easy poisoning, accelerating the degradation rate of the anode and decreasing the overall electrochemical performance of the fuel cell. In attempt to increase the oxidation of methane, the electrochemical performance of the cell, and decrease the carbon poisoning of the anode, VO_x/TiO_2 is introduced to the porous $LSB_{10}T$ /YSZ composite anode in small concentration. The presence of this catalyst inside anode enhances the catalytic activity of the anode, power and current density of the cell, and prevents the substantial formation of graphitic carbon and further carbon deposition on the surface of the anode.

3.2 Experimental procedure

3.2.1 Preparation of the catalyst

Commercially available TiO_2 (mixed anatase and rutile 99.5%, <100 nm, Aldrich) was intimately mixed in a solution of vanadium tri-isopropoxide in anhydrous dioxane to graft approximately 7 VOx/ nm^2, a monolayer of vanadium oxide onto TiO_2. The mixture was stirred continuously under inert atmosphere, at 25°C, for 48 h. Then, the solution was filtered to recover the solids, dried at 120 ºC and heated at 200 °C for 2 h. Finally, the dried solids were milled to form a fine powder and calcined at 500 °C for 5 h.

3.2.2 X-ray Photoelectron Spectroscopy

XPS analyses were performed for three different VOx/TiO_2 samples: fresh VOx/TiO_2 catalyst, VOx/TiO_2 catalyst after being exposed to air for 2 h at 800°C, and VOx/TiO_2 catalyst after being exposed sequentially to (CH_4, H_2S 0.5%) for 72 h and air for 2 h at 800°C. The binding energy of the O1s level was used for energy calibration as it is a better energy reference than the binding energy of C1s for establishing the V2p binding energies of vanadium oxides [11] since this binding energy is closer to V2p binding energy facilitating analyses of the spectra, and the V2p XPS signals were fitted by mixed Lorentzian–Gaussian curves using Casa XPS software.

3.2.3 Fourier Transform Infra-Red Spectroscopy

A Nicolet 8700 spectrometer was used to record the FTIR spectra of fresh VOx/TiO_2 catalyst powder at 25°C. The catalyst was previously dried and mixed with KBr.

3.2.4 X-Ray Diffraction

An X-ray diffract meter Siemens D5000 was used to determine the phases presented in VOx/TiO_2 and TiO_2. X-ray patterns were identified using Jade 5 software.

3.2.5 Catalytic Activity

A sampling valve and mass spectrometer (thermostat QMS 200) were situated close to the outlet of a flow rector made of quartz glass tube to analyze the exhaust gases and thereby monitor the catalytic activity at 800°C in three cases: 0.2 grams of VOx/TiO_2, 0.2 grams of TiO_2, and a quartz reactor containing no catalyst. The reacting gases consisted of CH_4 to (N_2, O_2 1%) , (CH_4, H_2S 0.5%) to (N_2, O_2 1%) ratios with various values at a flow rate of 50 mL min^{-1}.

3.2.6 SOFC preparation

Fuel cells were prepared by applying anode and cathode inks on to 1 cm^2 areas on opposed sides of commercial YSZ electrolyte pellets with a thickness of 300 μm. Equal amounts of commercial YZS (Tosho) and $LSB_{10}T$, which was prepared using solid state synthesis [5], were mixed with 5 wt. % of Polymethylmethacrylate (PMMA), milled and dispersed in glycerin to prepare the anode ink. To prepare the cathode ink, equal amounts of LSM and YZS (Tosho) were mixed, milled and dispersed in glycerin. The cell then was sintered at 1200°C for 1 h. For preparing the cell containing VO$_x$/TiO_2, the catalyst was adding after sintering by infiltrating a dilute suspension of VO$_x$/TiO_2 catalyst in ethanol into the composite YSZ and $LSB_{10}T$ anode to prepare a cell having an anode with approximately 1.5 wt. % supported VO$_x$ catalyst. Then, the cell was dried at 200 ºC for 2 h. To assemble the MEA, gold and platinum paste were printed on the anode and cathode sides of each cell, respectively, to collect the current of the cell, and the assemblies were sintered in situ at 900°C in flowing H_2 for 1 hour.

63

3.2.7 Potentiodynamic analyses

Potentiodynamic analyses were conducted using a Solatron instrument (SI 1287) without compensation with a scan rate of 5 mV s^{-1}. Pure H_2, H_2/0.5%H_2S and CH_4/0.5%H_2S were feed to the anode with a flow rate of 50 mL min^{-1} at 850 ºC and 900 ºC. The cathode side was exposed to air with the flow rate of 50 mL min^{-1}.

3.2.8 Potentiostatic determinations

Potentiostatic testing was conducted using the same Solatron instrument, without compensation, at 0.7 V and 850 ºC for 24 h using a gas mixture of CH_4/0.5%H_2S with a flow rate of 50 mL min^{-1}. The cathode side was exposed to air with the flow rate of 50 mL min^{-1}

3.2.9 Electrochemical impedance spectroscopy

Electrochemical impedance spectroscopy testing was carried out using a Solatron instrument (SI 1287) without compensation with a frequency range of 100000 Hz to 0.1 Hz and amplitude of 10 mV.

3.2.10 Scanning electron microscope (SEM)

Images of the anodic microstructure of the cell containing VO_x/TiO_2 before and after testing were examined using a scanning electron microscope (Hitachi S-2700).

3.2.11 Temperature programmed oxidation

After testing, the fuel cells were loaded in the TPO and exposed to 10% O_2/He with a flow rate of 50 mil/min during 1 hour for coking analysis. The temperature was incremented at a rate of 10K/min from room temperature to 1173 K. The composition of the exhausted gas was analyzed with a mass spectrometer (Cirrus, MKS spectra). TPO test of the cells was conducted by Dr. Singh and Dr. Hill at the University of Calgary.

3.3 Results and discussions

3.3.1 Material characterization

TiO_2 nanoparticles were successfully grafted with vanadium oxide, as evidenced by the peaks in the XPS spectra found for VO_x species on the surface of the support (Figure 3-1). Two peaks at 524.63 eV and 517.27 eV were attributed to the presence of vanadium with V 2p 3/2 and V 2p 1/2 respectively, corresponding to oxidation state 5+ (Figure 3-2). The position of the peak for V 2p 3/2, 517.2 eV, was consistent with an active phase comprising V_2O_5, isolated vandates, polyvanadates or a mixture of these species, each of which has oxidation state 5+.
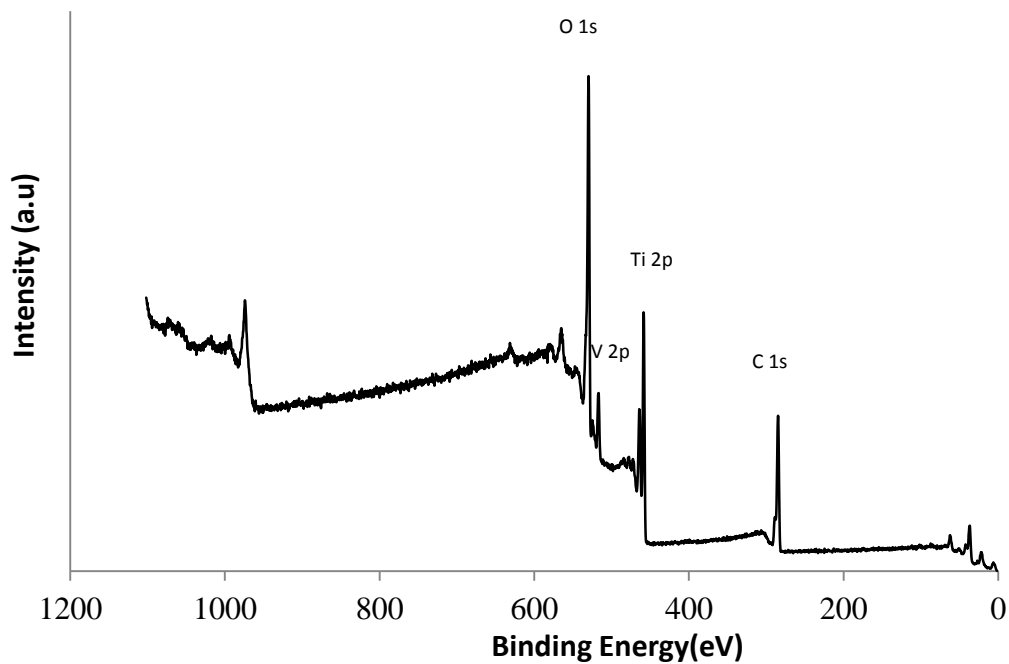
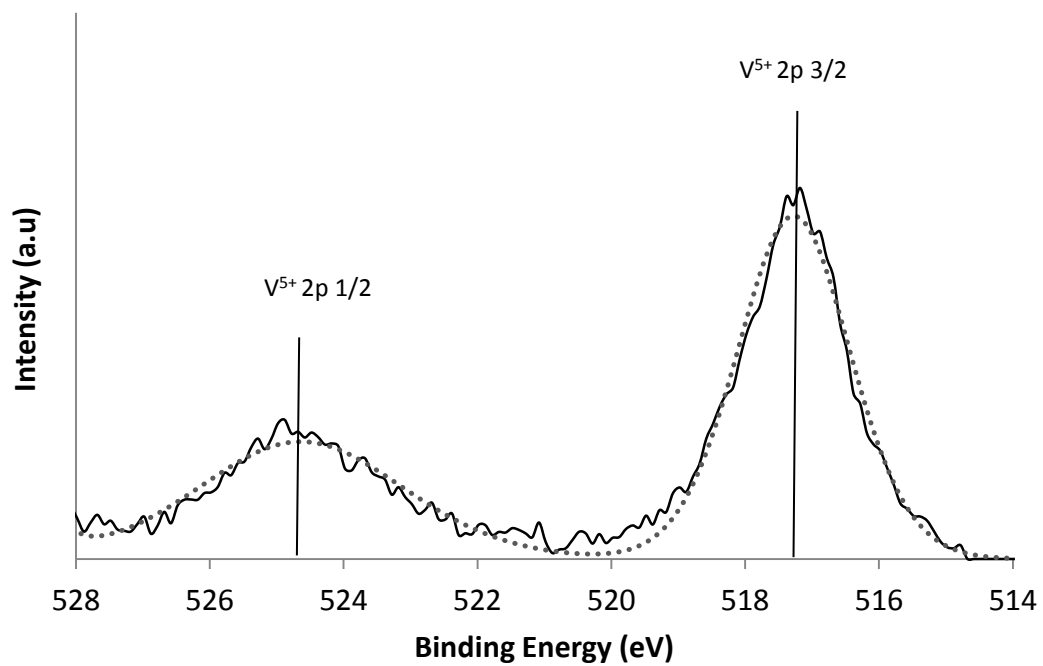**Figure 3-1 XPS of VO$_x$/TiO$_2$ after calcination at 500°C**

Figure 3-2 XPS of VO$_x$/TiO$_2$ after calcination at 500°C

Table 3-1 shows evidently the position of the peak of Ti 2p 3/2, 458.20 eV, and the atomic ratio (n_v /n_{Ti}) was about 0.16 for fresh VO_x/TiO_2, in good agreement with atomic ratios previously reported for vanadium supported on TiO_2 [11, 12]. The atomic ratio suggested also a good dispersibility of the active phase, providing more isolated vanadium species and so more available catalyst sites [8, 10].

	V 2p 3/2 (eV)	Ti 2p 3/2 (eV)	O 1s (eV)	n_v/n_{Ti} (Atomic ratio)
VO_x/TiO_2	517.27	458.2	529.8	0.16
VO_x/TiO_2	517.07	458.6	529.8	0.15
VO_x/TiO_2	517.13	458.2	529.8	0.21

Table 3-1 Atomic ratios of V and Ti from XPS

The active phase of vanadium was stable when the fresh catalyst was exposed to air at 800 °C for 2 h. The atomic ratio of this sample (Table 3-1) was similar to that reported for the fresh catalyst, and the activity was unchanged, showing that the vanadium phase and its dispersability were conserved on the surface of the support, TiO_2, even at this high temperature under oxidizing conditions. This confirmed the beneficial influence of the support on the thermal stability of the active phase of the catalyst.

On the other hand, the vanadium exhibited an oxidation state of 5+, shown by the peak at 517.13 eV, from the presence of either vanadates or V_2O_5 in the structure of the species on the support (Figure 3-3).
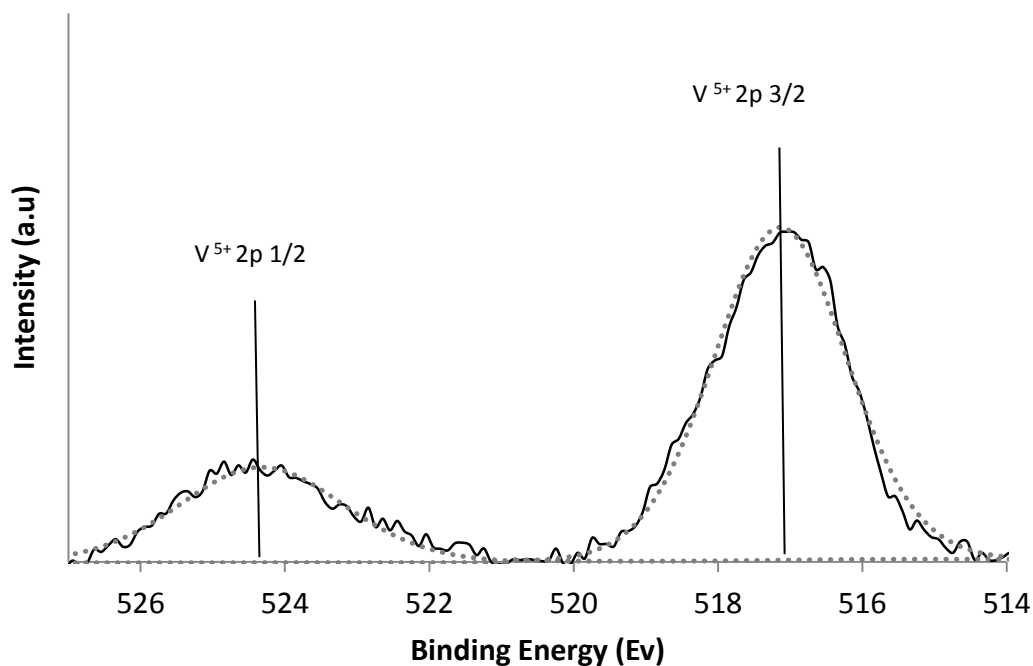
Figure 3-3 XPS of VO$_x$/TiO$_2$ after exposure to air for 2 h at 850°C

When the catalyst was exposed at 800 °C to sour methane for 3 days, and then to air for 2 h to remove the carbon deposited on the surface of the catalysts, the vanadium phase was stable, well dispersed on the support and did not evaporate due to either the high temperature or sulfidation of the active phase, based on the consistency of the vanadium peaks in the XPS spectra and atomic ratio V/Ti 0.15 (Table 3-1). Moreover, there were no peaks detected that could be assigned to sulfur, S 2s, S 2p, in the range 160 to 230 eV (Figure 3-4).
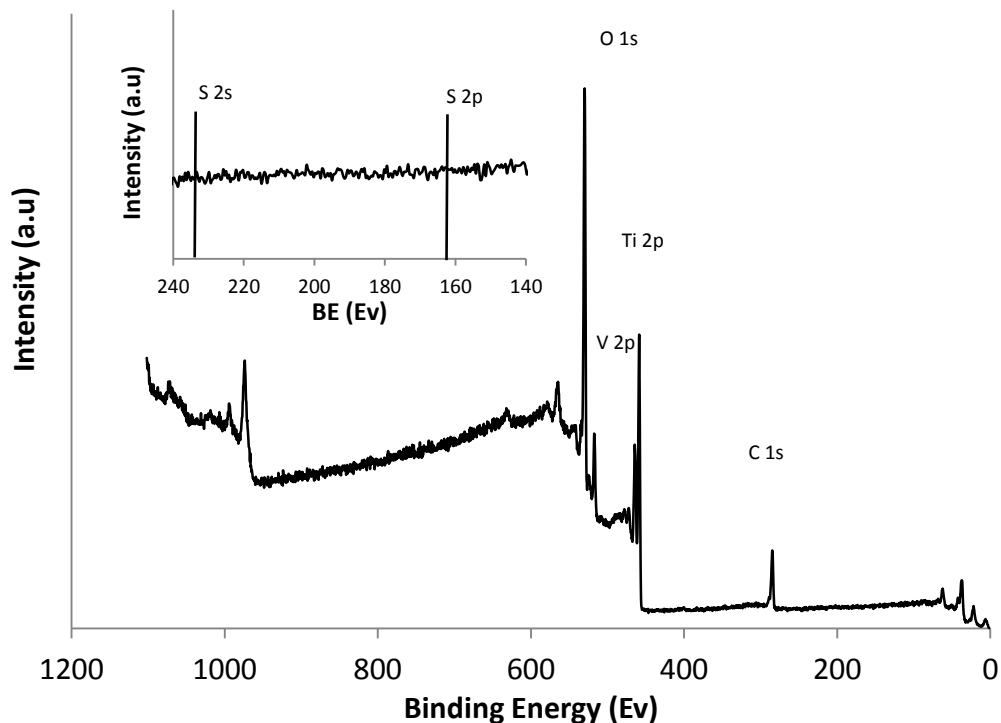
Figure 3-4 XPS of VO$_x$/TiO$_2$ after exposure at 850°C successively to methane containing 5000 ppm H$_2$S for 72 h and air for 2 h

There was an assymetric peak assignable to vanadium species in the range 516 eV to 520 eV (Figure 3-5). The presence of more than one oxidation state of vanadium caused the assymetry of the vanadium peak and the XPS spectra suggested the presence of vanadium in each of oxidation states 5+ and 4+. The exposure of the catalyst to reducing atmosphere, methane and H$_2$S, may have reduced a portion of the vanadium phase. The presence of vanadium species with oxidation state 4+ was indicated by the peak at 517.07 eV (Table 3-1), but the presence of VO$_2$ itself was considered highly unlikely since there was no peak in the range 515.6 to 516.02 eV attributable to this compound [11].
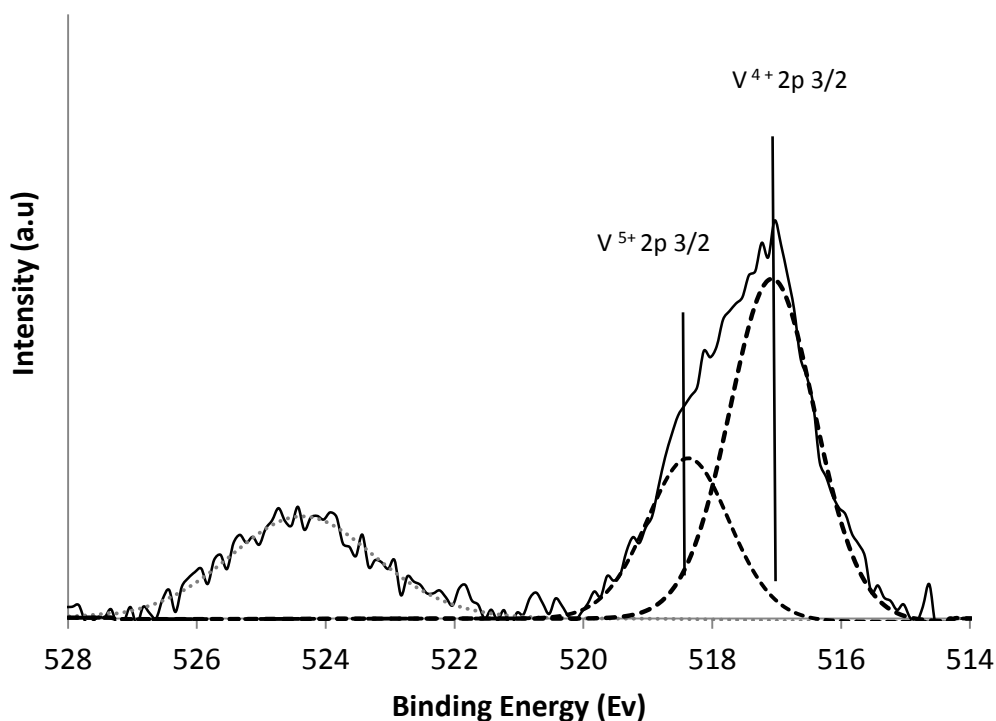
Figure 3-5 XPS of VO$_x$/TiO$_2$ after successive exposures to methane containing 5000 ppm H$_2$S for 72 h and air for 2 h

Figure 3-6 displays the vanadium and oxygen peaks of the three samples, calibrated using the oxygen peak at 529.8 eV. From this figure, the good stability of the sample exposed to sour gas and air is evident from the similarity of spectra exhibited by the fresh sample and the trated samples.

Except for the asymmetric peak of the sample exposed to sour gas and air, due to the partial reduction of the active phase when exposed to sour gas for 3 days, the two samples exhibited very similar intensity of the vanadium peak positions, suggesting similar concentrations of the surface species.
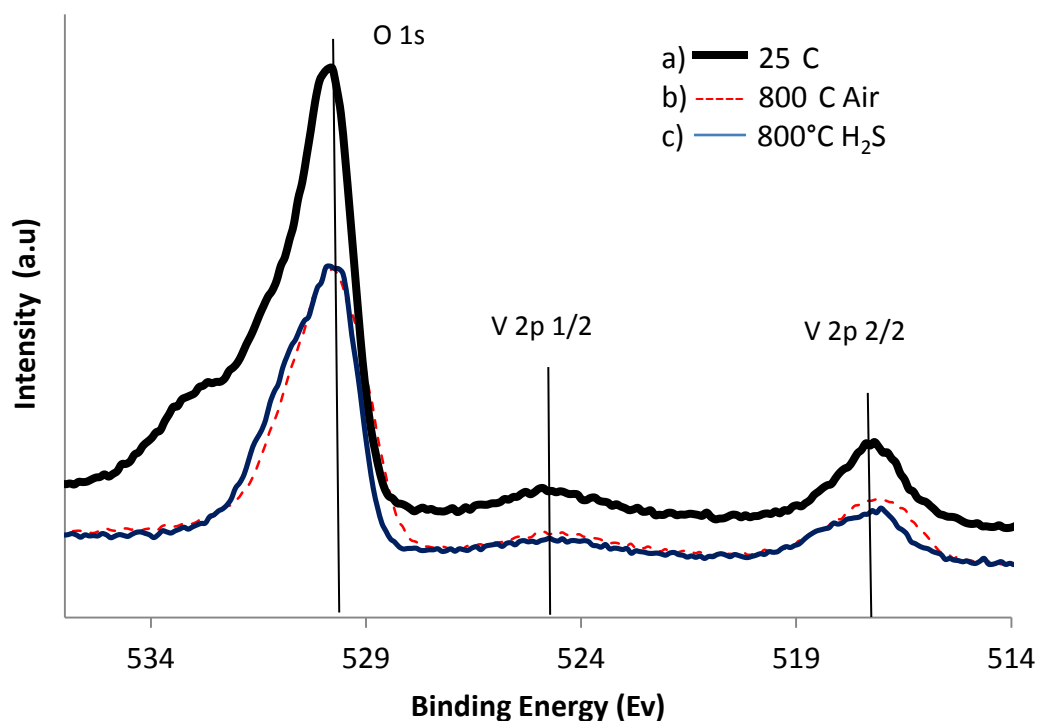
Figure 3-6 XPS of: a) VO$_x$/TiO$_2$ after calcination, b) VOx/TiO2 after exposure to air for 2 h, c) VO$_x$/TiO$_2$ after exposure successively to methane containing 5000 ppm H$_2$S for 72 h and air for 2 h

The XRD spectra of pure TiO$_2$ support showed evidently the presence of two different crystalline structures, anatase and rutile (Figure 3-7). When the support, TiO$_2$, was grafted with vanadium precursors and calcined at 500 °C, there were no additional discernible peaks in the XRD spectra of the grafted sample, showing that the active phase was well dispersed on the support (Figure 3-8). Owing to the low concentration of vanadium precursors used in the grafting process to achieve a monolayer of the active phase and isolated VO$_x$, it was not feasible to determine the exact form and structure of the active phase, VO$_x$, based on the XRD spectra of the grafted TiO$_2$ catalyst. Some small peaks at low

diffraction angles suggested the possible presence of V_2O_5 on the surface of the support. Similarly, the XRD spectra of the grafted support showed a mix of crystalline anatase and rutile phases even after calcination of the grafted support at 500 °C.
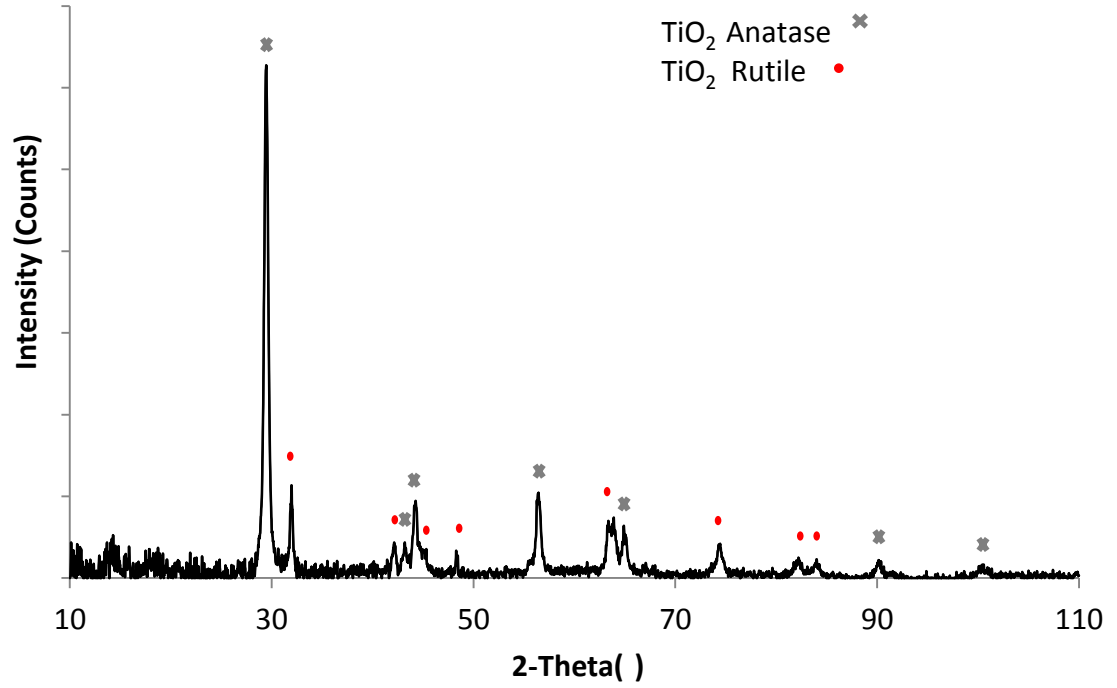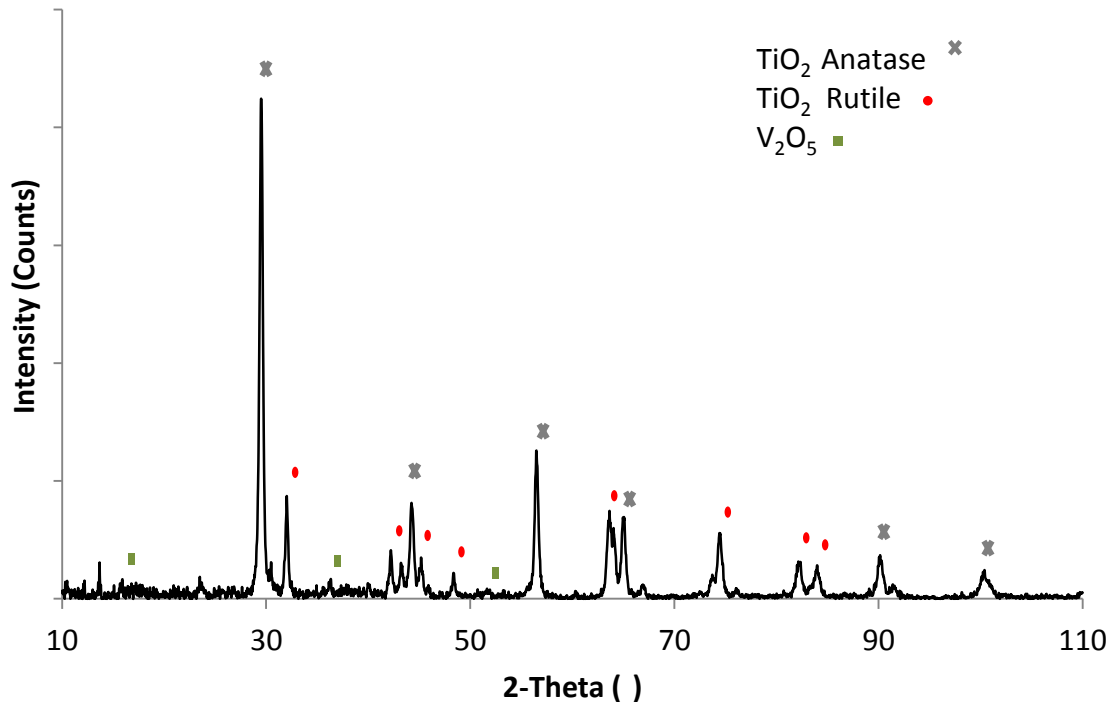

Figure 3-7 XRD of TiO₂

Figure 3-8 XRD of VO$_x$/TiO$_2$ after calcination at 500°C

The FTIR spectra of VO$_x$/TiO$_2$ showed the presence of a VO$_x$ phase on the surface of the support by four discrete peaks at 960, 1030, 1360 and 1610 cm$^{-1.}$ The bands at 960 and 1030 cm^{-1} were ascribed to the deformation and stretching vibrations of bonds V-O-V and V=O [14] (Figure 3-9). The small size of the peak at 960 cm^{-1} was due to the high dispersibility of VO$_x$ and its low concentration. The peak at 1030 cm^{-1} was within the range 1010- 1036 cm^{-1} attributable to the stretching mode of VO$_x$ units, isolated vanadium species, or the V-O stretching mode of VO$_x$ clusters. A small peak at 1360 cm^{-1} was attributable to one or the combination of the anatase phase of the support and the V-O bending mode [13]. The remaining peak in this group, at 1610 cm^{-1}, was ascribed to the overtone of

the bond V-O-V and/or the presence of a small amount of unreacted isolated hydroxyl groups remaining on the support after calcination [13].
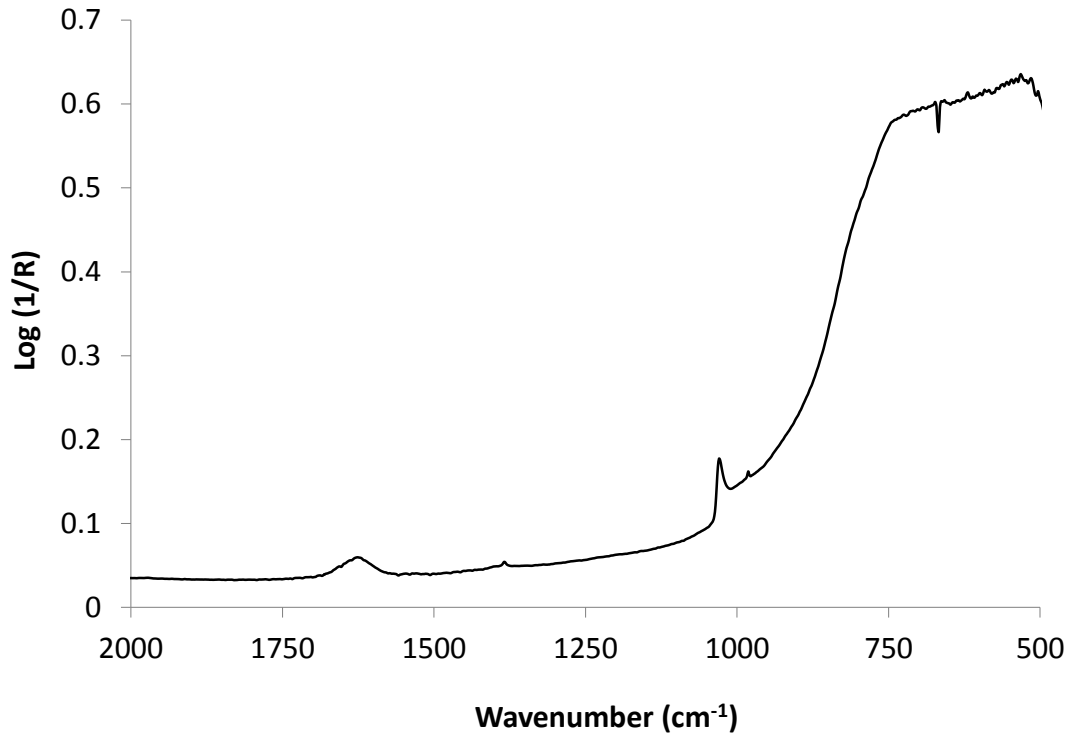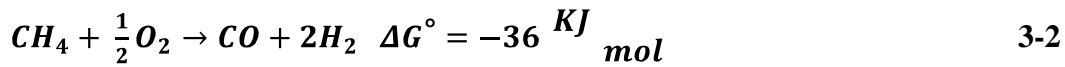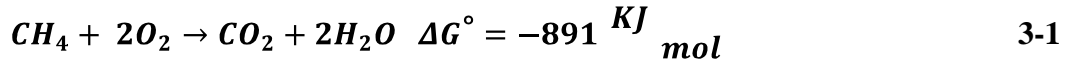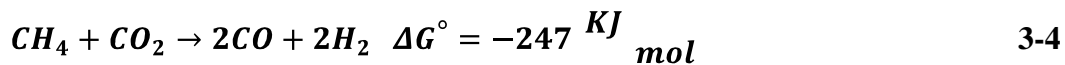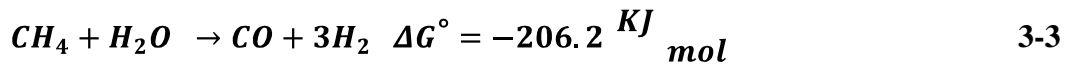

Figure 3-9 FTIR of VO$_x$/TiO$_2$ after calcination at 500°C

3.3.2 Chemical activity characterization

There have been reported some reaction for reforming and oxidation of methane. Reactions 3-1 and 3-2 show the complete and partial oxidation of methane respectively which maybe occur in my system:

$$CH_4 + 2O_2 \rightarrow CO_2 + 2H_2O \quad \varDelta G° = -891 \; \frac{KJ}{mol} \qquad\qquad \text{3-1}$$

$$CH_4 + \frac{1}{2}O_2 \rightarrow CO + 2H_2 \quad \varDelta G° = -36 \; \frac{KJ}{mol} \qquad\qquad \text{3-2}$$

Similarly, secondary reactions might be involved and promote reforming of the fuel. Reaction 3-3 and Reaction 3-4 depict the steam and dry reforming of methane respectively:

$$CH_4 + H_2O \; \rightarrow CO + 3H_2 \quad \varDelta G° = -206.2 \; \frac{KJ}{mol} \qquad\qquad \text{3-3}$$

$$CH_4 + CO_2 \rightarrow 2CO + 2H_2 \quad \varDelta G° = -247 \; \frac{KJ}{mol} \qquad\qquad \text{3-4}$$

Finally, side or intermediate species may react, extending the possible routes and reactions. As for example, Reaction 3-5 which shows the well-known water-gas shifts reaction:

$$CO + H_2O \; \rightarrow CO_2 + H_2 \quad \varDelta G° = -41.2 \; \frac{KJ}{mol} \qquad\qquad \text{3-5}$$
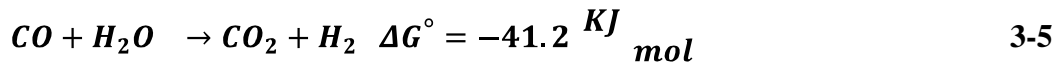
In the following catalytic characterization study, a mass spectroscopy was used to measure the ion current of the most representative products, CO, CO_2 and H_2O, of the catalytic combustion and reforming of methane and sour gas.

A flow reactor filled with either 0.2 g of VO_x/TiO_2 or TiO_2 catalyst exhibited higher production of H_2O at 800 ˚C than that achieved when the reactor had no catalyst, for which the extent of reaction was that anticipated from

thermodynamics or thermal driving forces (Figure 3-10). Thus the reactor itself was inactive, and each of TiO_2 alone and TiO_2 supported VO_x were active for oxidation of H_2 produced from the methane.
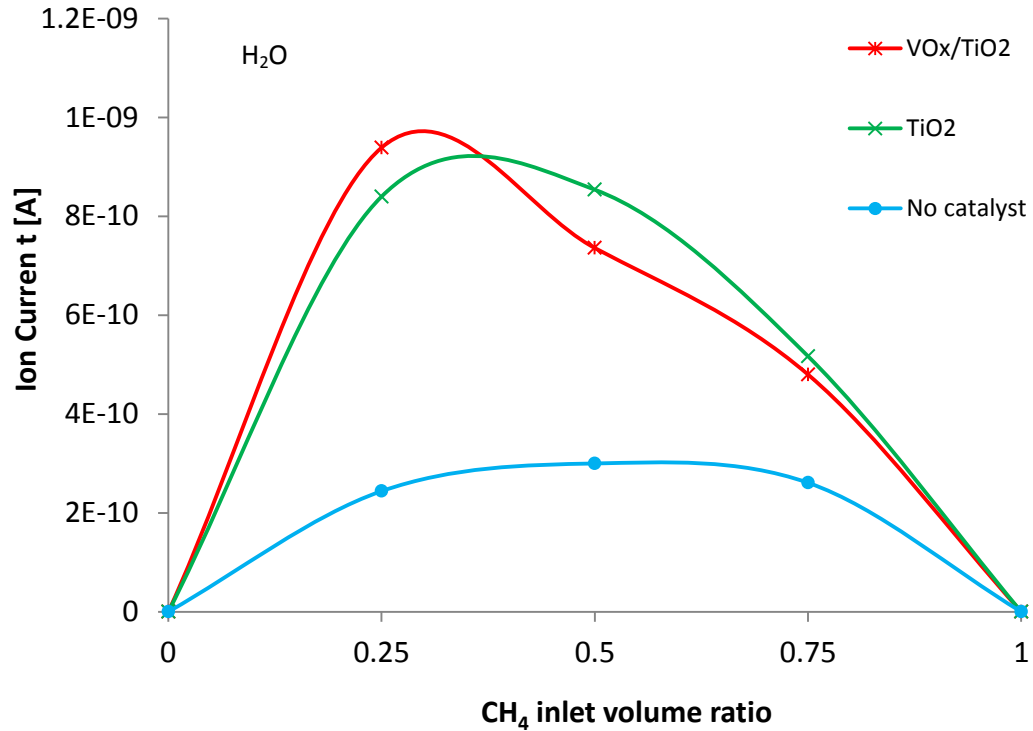

Figure 3-10 Production of H_2O

When TiO_2 was the catalyst the production rate of CO increased and the production of CO was higher than that exhibited in the system when the catalyst was VO_x/TiO_2, also at 800 ˚C (Figure 3-11). Based on the ion currents generated, each of TiO_2 and VO_x/TiO_2, enhanced the oxidation rate of methane and production rate of CO from methane. In addition, at lower CH_4 to (N_2, O_2 1%)

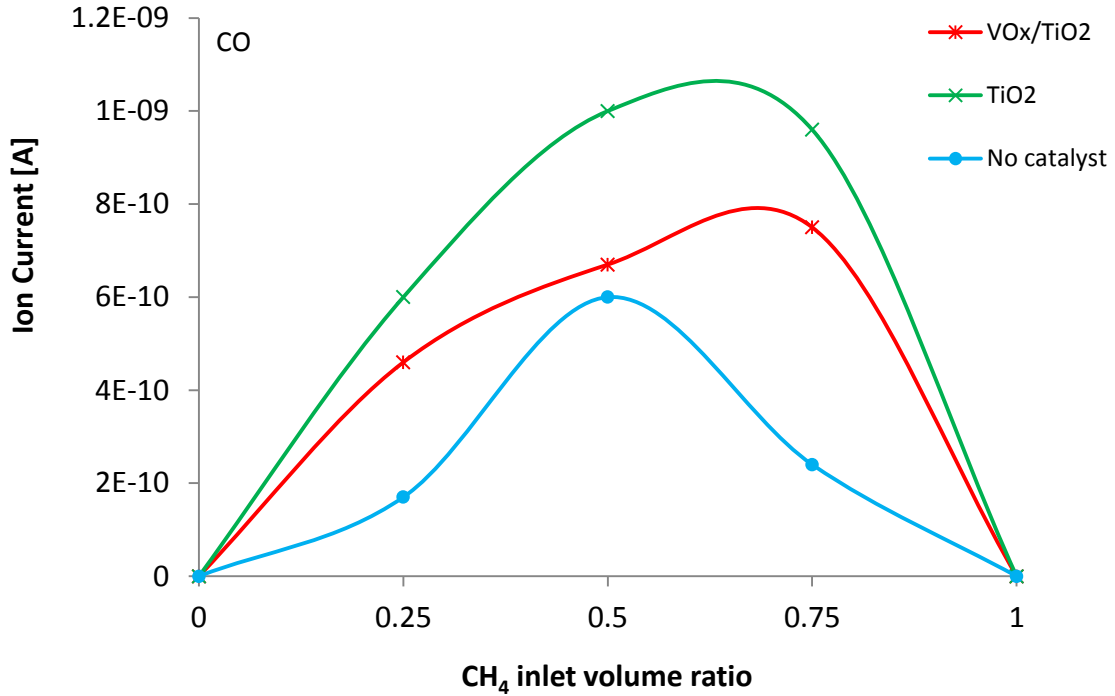ratio, the rate of partial oxidation of methane to produce CO increased (Figure 3-2).

Figure 3-11 Production of CO

VO_x/TiO_2 is active for complete oxidation of methane to CO_2 (Figure 3-12). The maximum rate of production of CO_2 was achieved when the ratio of methane to oxygen balanced with helium was about 0.25. At high CH_4 to (N_2, O_2 1%) ratio and H_2O production, the complete oxidation of methane increased, producing more CO_2. However, the role of H_2O in the reaction process cannot be determined unequivocally from the present data. VO_x/TiO_2 promoted a

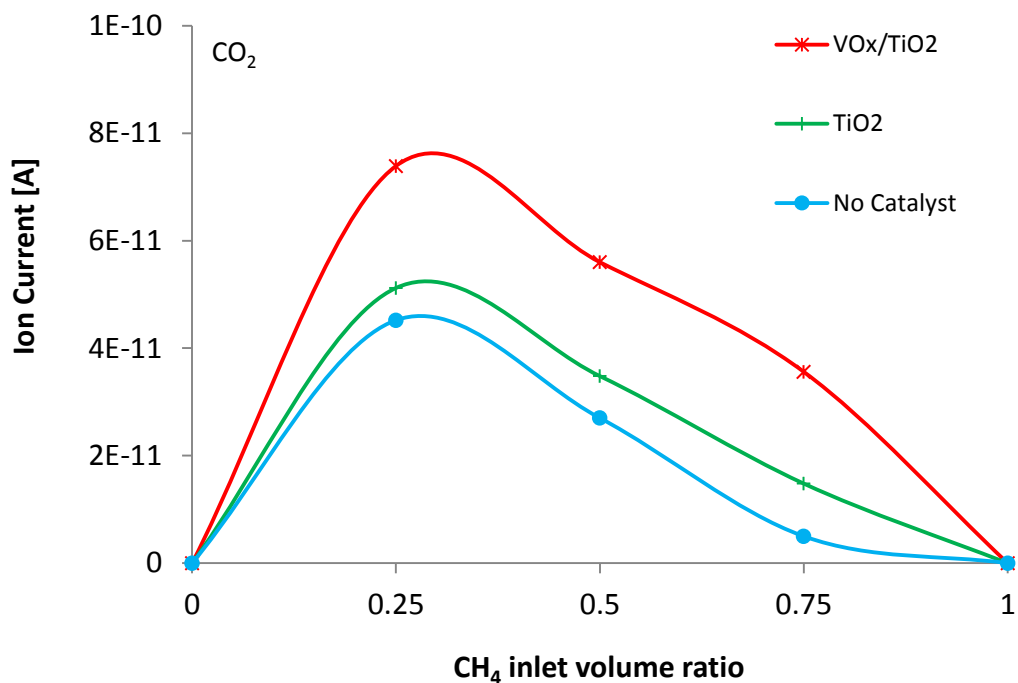considerably higher production rate of H_2O than those of TiO_2 as catalyst and the system without any catalyst.

Figure 3-12 Production of CO_2

The production of H_2O when VO_x/TiO_2 was exposed to sour gas, methane with 5000 ppm of H_2S, was similar to the production of H_2O when methane without H_2S was used as reactant, showing that this catalyst was chemical stable in the presence of H_2S under these conditions (Figure 3-13). In contrast, comparing Figure 3-13 with Figure 3-10, it is noticeable the detrimental effect of H_2S on catalytic performance of TiO_2. Thus there was a beneficial catalyst-support interaction between the components of VO_x/TiO_2.
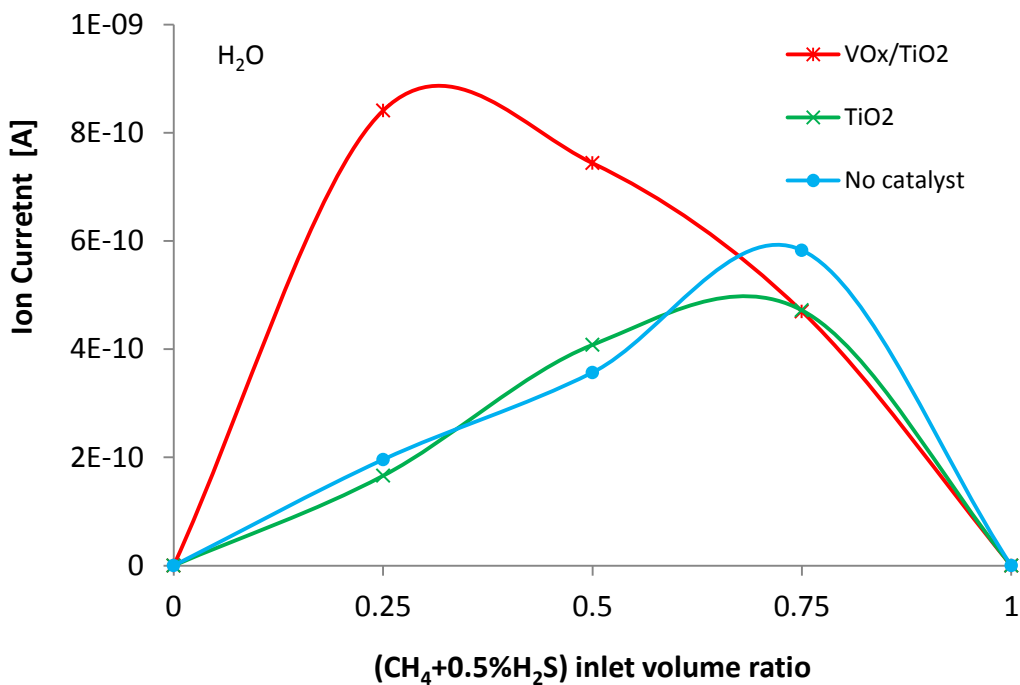
Figure 3-13 Production of H₂O in the presence of H₂S

When the reactor was either unpacked or packed with TiO_2, there were no substantial CO productions whereas significant amounts of CO were produced over VOx/TiO_2 (Figure 3-14). The amount of CO production was comparable to that when VOx/TiO_2 was exposed to methane without H_2S. Furthermore, the active phase of the catalyst, VO_x, was stable at this concentration and fostered the oxidation of methane even in the presence of the high concentration of H_2S.
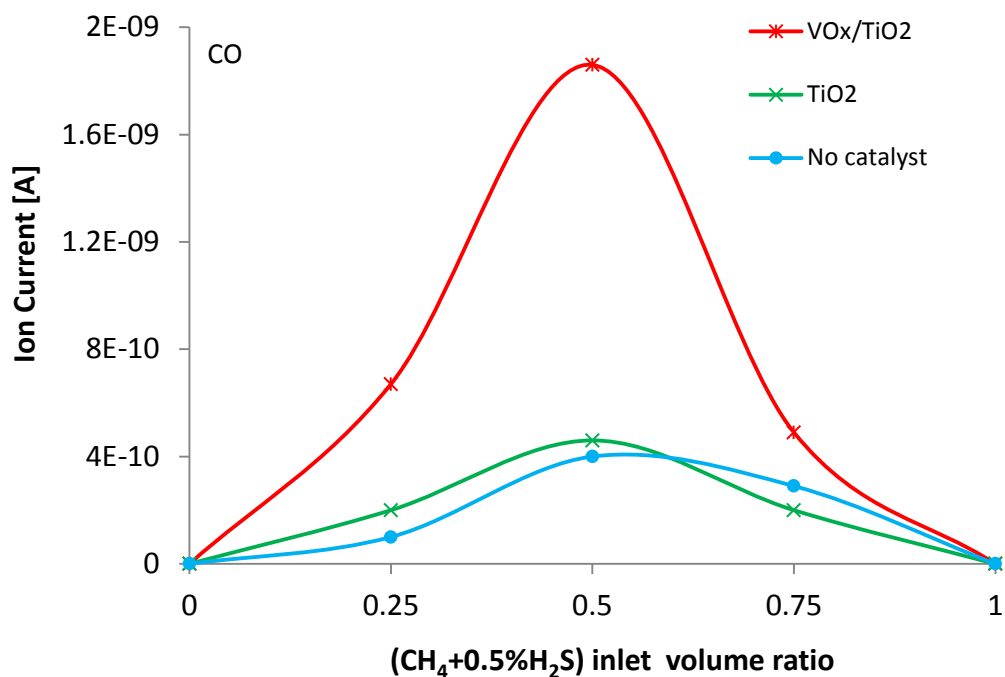
Figure 3-14 Production of CO in the presence of H₂S

Figure 3-15 also shows that VOx/TiO$_2$ was active for the complete oxidation of sour gas even when there was a high concentration, 5000 ppm, of H$_2$S. In contrast, the packed reactor with TiO$_2$ and the unpacked reactor had lower conversion rates and production of CO$_2$. The relatively lower production of CO$_2$ confirmed that the catalytic activity of TiO$_2$ was affected by the presence of H$_2$S, possibly due sulfur formation and deposition on this catalyst at this concentration of H$_2$S and temperature.
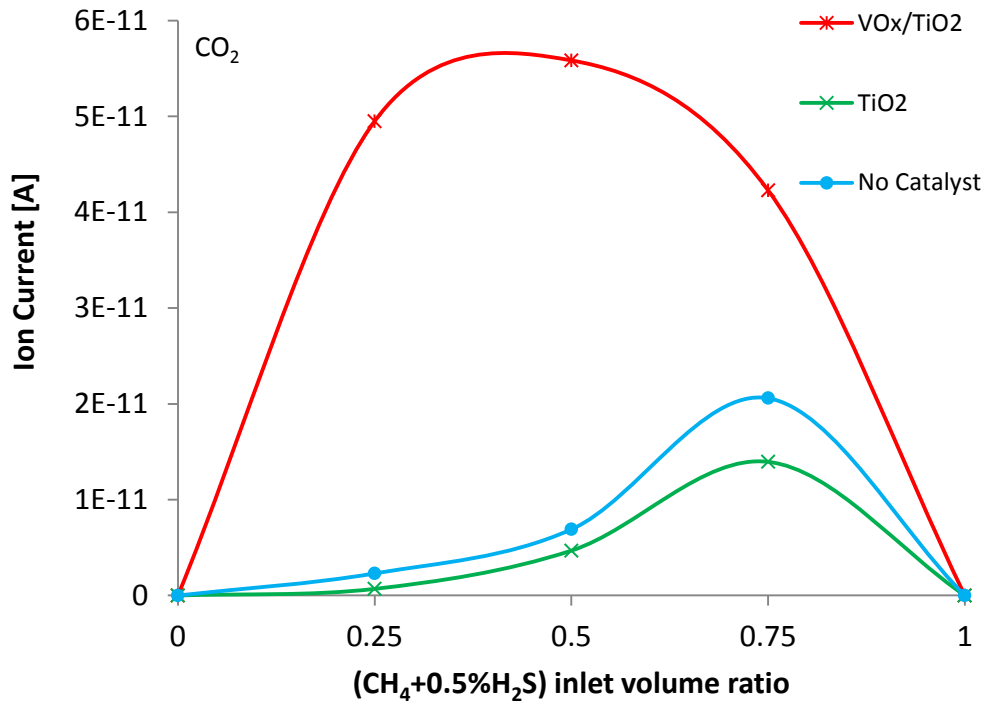
Figure 3-15 Production of CO$_2$ in the presence of H$_2$S

3.3.3 Fuel cell characterization

When the catalyst was infiltrated into the anode, VO$_x$/TiO$_2$ resided mainly on the surface of the LSB$_{10}$T and YSZ matrix due to the distribution of its particle size and based on SEM images taken to the cross section of the anode before and after the fuel cell test. In both cases the microstructure exhibited good porosity, contact between LSB$_{10}$T and YSZ, and adhesion of the anode and electrolyte (Figure 3-16).
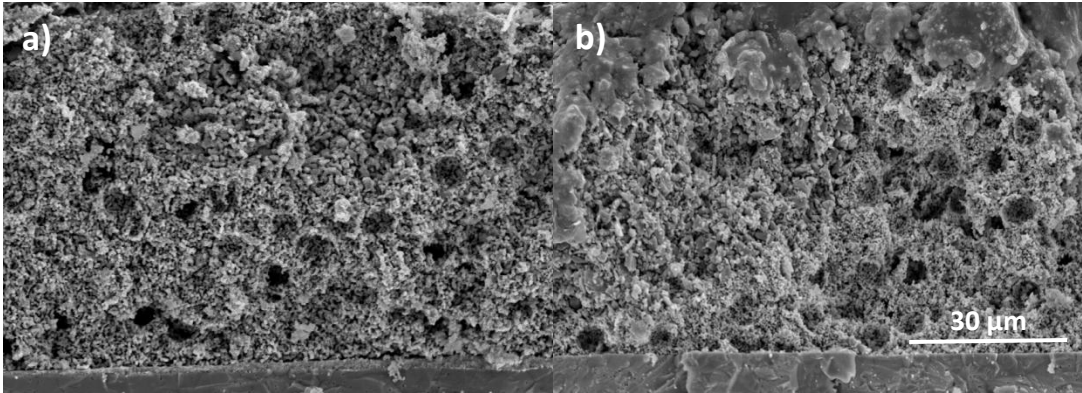
Figure 3-2 Anodic microstructure of the cell with VO$_x$/TiO$_2$; a) Before and b)after fuel cell test.

The anode with VO$_x$/TiO$_2$ had higher performance and increased the power density by 25 % compared to a sample with an anode comprising only LSB$_{10}$T and YSZ at either 850 or 900°C (Figure 3-17). It is also obvious from the pontentiodynamic tests at 850°C and 900°C, the positive effect of the temperature on the performance of the fuel cells.

The power density enhancement is attributed to the presence of VO$_x$/TiO$_2$ which helped to faster oxidize and produced compounds such as CO from the partial oxidation of sour gas. It is also believed that the content of H$_2$S in the feed foments the oxidation of methane, facilitating a higher electrochemical reaction rate at the (TPB).
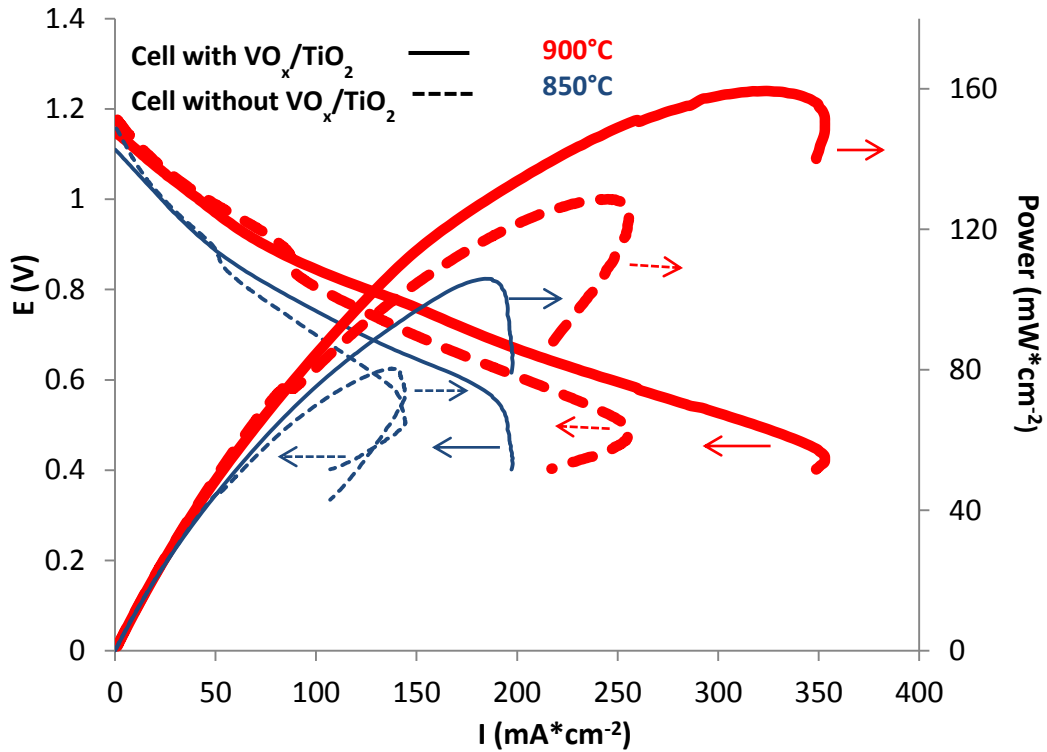
Figure 3-3 Potentiodynamic tests at 850°C and 900°C of fuel cells fed with methane containing 5000 ppm of H₂S

From Figure 3-17, it is obvious that the introduction of the catalyst reduced mass transfer resistance at low voltages. This effect is attributed to the rapid oxidation of carbon during the thermal cracking of methane and severe heat conditions, avoiding formation of carbon entities on the surface of the anode, blocking of the pores and deactivation. Furthermore, the good stability of the catalyst in high concentration of H₂S also reduced any propensity to sulfur deposition without sulfidation and evaporation of the active phase. Potentiostatic tests conducted on the fuel cells showed the good stability of the anodes over 24 h

using as feed methane containing 5000 ppm of H_2S at 850 °C, when the cell was
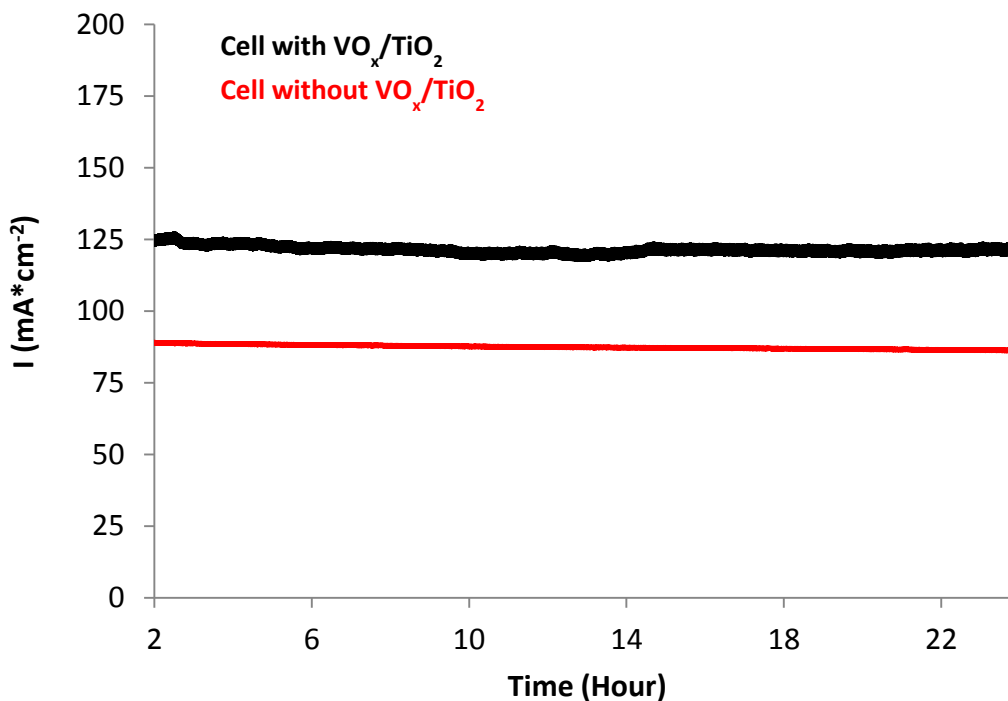
operated with a bias of 0.7 V (Figure 3-18).

Figure 3-4 Potentiostatic stability tests at 850°C and 0.7 V in methane containing 5000 ppm H_2S

TPO analysis conducted on the cells confirmed the good coking tolerance

of the fuel cell with VO_x/TiO_2 (Figures 3-19 and 3-20). Significant lower ratio of

graphitic carbon to reactive carbon was found when the anode contained

VO_x/TiO_2 due to the good oxidizing activity of the catalyst, promoting the CO,

CO_2 production, and less graphitic carbon formation which is hard to remove from

the surface of the anode due to its lack of reactivity, high stability and tendency to

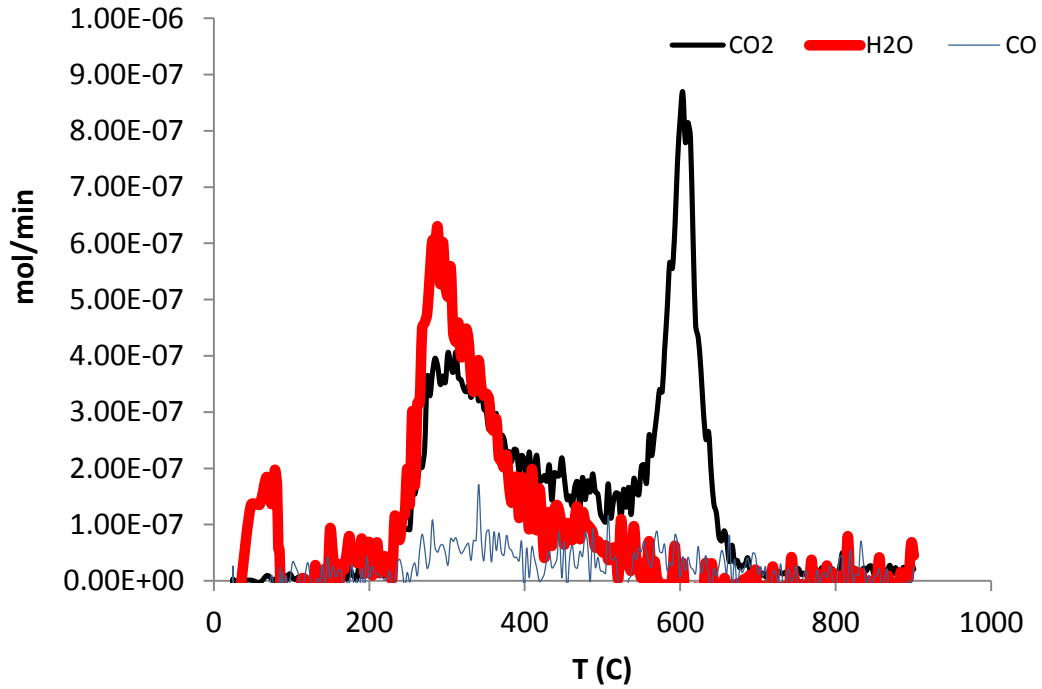block the surface, reducing the fuel diffusivity and activity of the anode.
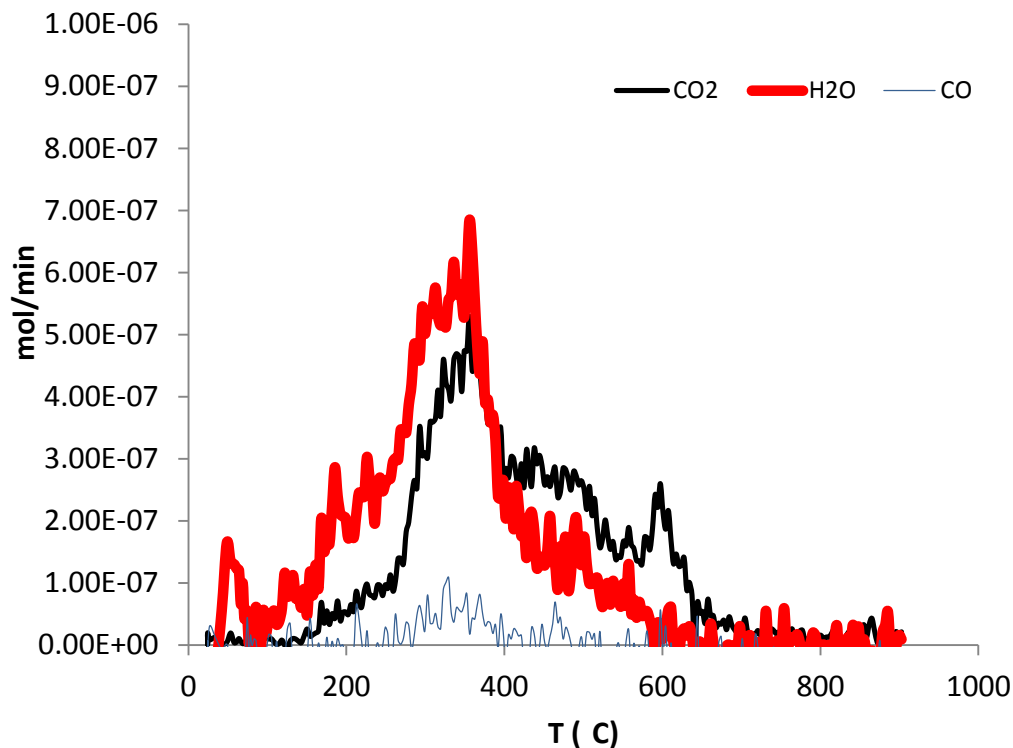

Figure 3-5 TPO analysis of the composite anode, LSB$_{10}$T and YSZ

Figure 3-6 TPO analysis of the composite anode, LSB$_{10}$T and YSZ containing VO$_x$/TiO$_2$

I-V and I-P curves of different samples in sour gas illustrated the complexity and high catalytic activity of the system when the feed contained a 5000 ppm of H$_2$S (Figure 3-17). When sulfur tolerant materials comprise the anode, H$_2$S does not poison the material and helps to oxidize methane, producing more electro active compounds as CO or COS, compounds that are easier adsorbed on the surface and electrochemically oxidized at the TPB. Roushanafshar et al. proposed that the presence of H$_2$S enhances the performance of the cell by reacting with CO and final regeneration of H$_2$S [14].

Reactions 3-6 and 3-7 show the thermodynamic feasibility for oxidation of sour gas, production of carbon monoxide, CO, and H_2S regeneration at 850°C. Similarly, Reactions 3-8, 3-9 and 3-5 show the thermodynamic feasibility for production of carbonyl sulfide, COS, with H_2S regeneration. Nevertheless, this last mechanism is less likely than CO production based on the thermodynamic predictions. On the other hand, the I-P curve showed a sudden power drop from intermediate to low potential values (Fi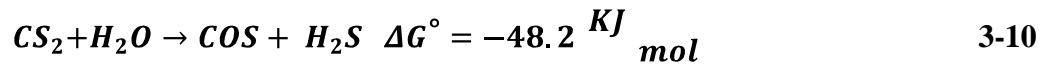gure 3-17). This abrupt power drop was attributed to the consumption and oxidation of H_2S, producing either CS_2 or SO_2 [15]. The H_2S consumption reduces the chemical and electrochemical oxidation rate of the fuel, dropping dramatically the current and power density of the cell. In addition, H_2S consumption makes more severe the carbon deposition, leading to a faster degradation of the anode. Reactions 3-9 and 3-10 show the mechanism for which carbon deposition might be reduced in presence of H_2S, and H_2S regeneration.

Production of electro active specie, CO, and H_2S regeneration

$$O_2 + H_2S \rightarrow SO_2 + H_2O \quad \Delta G° = -430.7 \; \frac{KJ}{mol} \qquad \qquad \text{3-6}$$

$$SO_2 + CH_4 \rightarrow H_2S + CO + H_2O \quad \Delta G° = -184.7 \; \frac{KJ}{mol} \qquad \qquad \text{3-7}$$
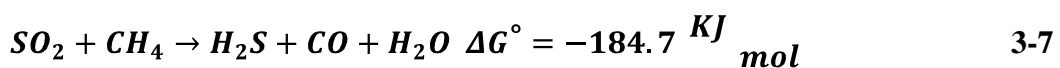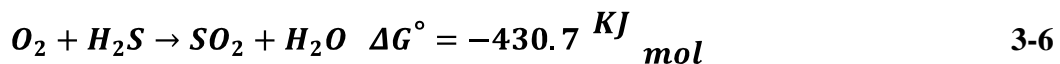
Production of electro active specie, COS, and H_2S regeneration

$$O_2 + H_2S \rightarrow \frac{1}{2}S_2 + H_2O \quad \Delta G° = -301.5 \; \frac{KJ}{mol} \qquad \qquad \text{3-8}$$

$$S_2 + C \rightarrow CS_2 \quad \Delta G° = -181 \; \frac{KJ}{mol} \qquad \qquad \text{3-9}$$

$$CS_2 + H_2O \rightarrow COS + H_2S \quad \Delta G^\circ = -48.2 \; \frac{KJ}{mol} \qquad \text{3-10}$$
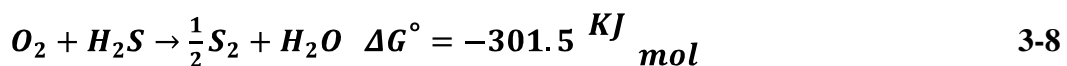
To study the role of VO_x/TiO_2 in other feeds, the fuel cell was fueled with pure H_2 and H_2 containing 5000 ppm of H_2S at 850°C and 900°C. Figure 3-21 shows higher performances and electrochemical conversions of the cell when H_2 and H_2 containing H_2S were used as fuels than the performance depicted by the fuel cell when it was fuelled with methane containing H_2S at 850°C and 900°C. The higher electrochemical conversion is attributed to the high electro activity of hydrogen which is easier to electrochemically oxidize than methane and to the oxidizing role of the catalyst, $VO_x/TiO_{2,}$ which helps to further oxidize this element and foster higher electrochemical oxidation rates.

In addition, the power density of the fuel cell increased with sour gas. It is believed that H_2S is oxidized enhancing the current and power density of the fuel cell. H_2S might also promote higher electro activity of H_2 without H_2S consumption by an unclear mechanism yet.
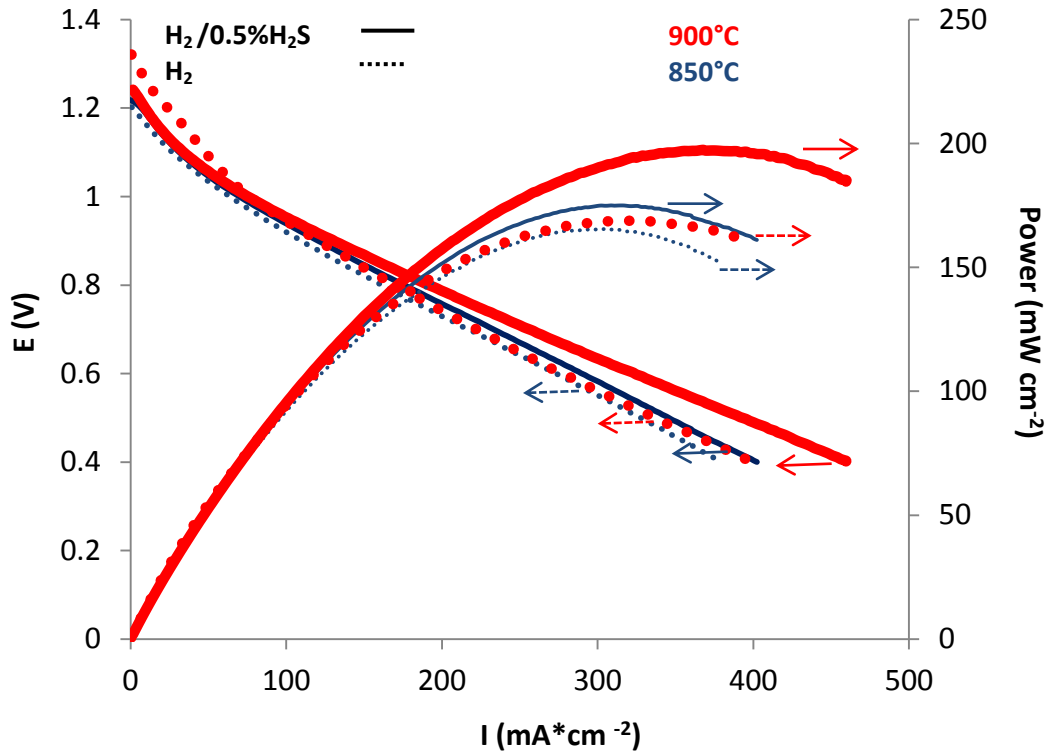
Figure 3-7 Potentiodynamic tests at 850˚C and 900°C of the cell with VO$_x$/TiO$_2$ fed with hydrogen and hydrogen containing 5000 ppm of H$_2$S

An electrochemical impedance spectroscopy test, EIS, conducted on the fuel cell containing VO$_x$/TiO$_2$ using H$_2$, H$_2$ containing 5000 ppm of H$_2$S and methane containing 5000 ppm of H$_2$S revealed the positive effect of H$_2$S on the polarization resistance (Figure 3-22). When the gas was switched from pure H$_2$ to H$_2$ containing 5000 ppm H$_2$S, the polarization resistance decreased, suggesting easier oxidation of H$_2$ at the anode and good sulfur tolerance. Switching the feed to methane containing 5000 ppm of H$_2$S, the polarization resistance increased due to the poorer electro activity of methane.

Generally speaking, the low Rp values are also attributed to the good microstructure with large number of TPBs that maximize the electrochemical reactions and electrochemical oxidation of the fuel.

On the other hand, the ohmic resistances (high frequency intercept), Rs, were low in all the experiments and the composite anode exhibited relatively good conductivity and contact with the current collector. Regarding the conductivity of the VO_x/TiO_2, this compound is rather considered a non-conducting material when the active phase of the catalyst exhibits an oxidation state 5+. Nevertheless, the concentration of the catalyst was low enough and the particles were well dispersed on the surface of the anode in order to avoid significant ohmic resistance.
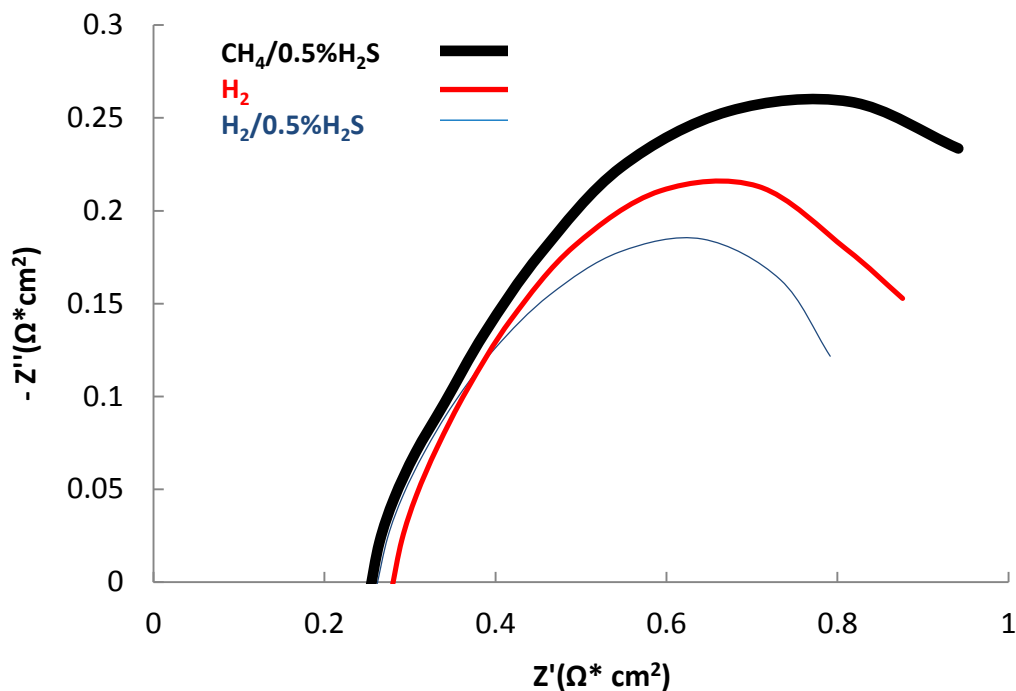
Figure 3-8 EIS of the cell VO$_x$/TiO$_2$ fed with hydrogen, hydrogen containing 5000 ppm H$_2$S and methane containing 5000 ppm H$_2$S at 850°C

3.4 Conclusions

Vanadium oxide, VO$_x$, was successfully deposited on the surface of TiO$_2$ with the grafting method. VO$_x$ phase grafted onto TiO$_2$ comprised mainly vanadate species, characterized using XPS, XRD and FTIR.

XPS showed that the active phase was stable at temperatures to at least 800°C in an oxidizing environment. When high concentration of H$_2$S, 5000 ppm, was present there was no sulphidation of the active phase. There was evidence of reduction of a portion of the vanadium in the active phase from 5+ to 4+ when exposed to methane containing H$_2$S. While the small concentration of the active

phase in VO_x/TiO_2 made it difficult to discern small new peaks in the XRD spectra of the grafted TiO_2, and so no definitive conclusions can be drawn from XRD data, the FTIR data showed small peaks assignable to the vibrations of the bonds V-O-V and V=O of vanadate species containing both oxidation states 5+ and, in lesser amount, 4+.

The presence of H_2S did not affect the chemical activity of the VO_x/TiO_2 for partial oxidation and complete oxidation of methane to carbon monoxide and carbon dioxide respectively. The production of H_2O during this reaction also increased the production and selectivity to carbon monoxide.

$LSB_{10}T$ mixed with YSZ had good stability in methane containing 5000 ppm of H_2S and the performance was improved when the mixture also contained VO_x/TiO_2. The power density enhancement is attributed to the strong oxidizing role of the catalyst and good cooking tolerance. Potentiostatic tests showed the good stability in 5000 ppm H_2S. The presence of H_2S in the feed increased the performance of the cell and decrease the polarization resistance when sulfur tolerant composite anode are used, making sour gas a potential fuel for SOFCs.

References

[1] M. Gong, X. Liu, J. Trembly, C. Johnson, J.Power Sources, 168 (2007) 289-298.

[2] J.B. Goodenough, Y. Huang, J.Power Sources, 173 (2007) 1-10.

[3] J.W. Fergus, Solid State Ionics, 177 (2006) 1529-1541.

[4] Z. Cheng, S. Zha, L. Aguilar, M. Liu, Solid State Ionics, 176 (2005) 1921-1928.

[5] A. Vincent, J. Luo, K.T. Chuang, A.R. Sanger, J.Power Sources, 195 (2010) 769-774.

[6] I.E. Wachs, Catalysis Today, 100 (2005) 79-94.

[7] F. Arena, F. Frusteri, A. Parmaliana, Applied Catalysis A: General, 176 (1999) 189-199.

[8] G.C. Bond, S.F. Tahir, Applied Catalysis, 71 (1991) 1-31.

[9] A. Sorrentino, S. Rega, D. Sannino, A. Magliano, P. Ciambelli, E. Santacesaria, Applied Catalysis A: General, 209 (2001) 45-57.

[10] G.C. Bond, Applied Catalysis A: General, 157 (1997) 91-103.

[11] G. Silversmit, D. Depla, H. Poelman, G.B. Marin, R. De Gryse, Journal of Electron Spectroscopy and Related Phenomena, 135 (2004) 167-175.

[12] M. Cozzolino, R. Tesser, M. Di Serio, M. Ledda, G. Minutillo, E. Santacesaria, Studies in Surface Science and Catalysis, 106 (2006) pp. 299-306.

[13] K.V. Narayana, A. Venugopal, K.S. Rama Rao, S. Khaja Masthan, V. Venkat Rao, P. Kanta Rao, Applied Catalysis A: General, 167 (1998) 11-22.

[14] M. Roushanafshar, J. Luo, A.L. Vincent, K.T. Chuang, A.R. Sanger, Int J Hydrogen Energy, 37 (2012) 7762-7770.

[15] A.L. Vincent, J. Luo, K.T. Chuang, A.R. Sanger, Applied Catalysis B: Environmental, 106 (2011) 114-122.

Chapter 4   Conclusion and recommendations

The composite anode $LSB_{10}T$/YSZ exhibits relatively good tolerance and activity for electrochemical oxidation of different fuels including sour gas, methane containing 5000 ppm of H_2S. In this kind of anode all the catalytic activity relies on the action of $LSB_{10}T$ and presence of barium in the perovskite. Keeping high conductivity and activity is rather difficult and this perovskite turns out being a material which helps to enhance the electronic conductivity rather than the catalytic activity of the composite anode. Similarly, the presence of YSZ helps to increase the ionic conductivity of the composite anode but doesn't contribute to the improvement of the catalytic activity. For this reason, proposing a single phase and compound for SOFC anode with good electronic, ionic and catalytic activity has become in a difficult task.

The addition of components that enhance a specific property is a different alternative to optimize it and achieve a better performance. In order to carry out this engineering and scientific task, it is necessary to know in details each compound of the anode as their reactivity, operating conditions, properties and roles. As an example, V_2O_5 is a good catalyst for oxidation reactions but it's not stable in presence of O_2 or H_2S at high temperature range. Even though, reduction of vanadium oxide, 5+ to 4+, might increase the stability and electronic conductivity but decreases the catalytic activity. VO_x/TiO_2 is a different story, small concentration of vanadium grafted on the surface of titanium oxide are

94

stable at high temperatures with an oxidation state +5 which enhance the oxidizing activity of the anode.

Addition in small concentration of VO_x/TiO_2 to $LSB_{10}T/YSZ$ composite anode increases the power density and stability by accelerating the production of CO for its further electrochemical conversion and promoting the production of CO_2 respectively. Selectivity for CO or CO_2 can be a parameter should be considered for getting a better effect on either the stability or power output of the anode depending on the objective. To play with the selectivity, parameter as concentration of precursor and pH should be considered during the synthesis and grafting process of the catalyst.

Smaller VO_x/TiO_2 particles are desirable, not only to have a uniform distribution and microstructure but also to increases the TPB. VO_x/TiO_2 phase should not be considered as part of the TPB, since TPB is the point where an active gas is in contact with an ionic and electronic phase to be electrochemically oxidized and VOx/TiO_2 is neither in gas state or a good conductor. However, smaller VO_x/TiO_2 particles increase the surface area of the catalyst increasing the concentration of active gases at the TPB.

Also the particle size improves the impregnation of the catalyst deeper inside the anode and at the active layer next to the electrolyte. The results of the present work show that presence of the catalyst on the surface is beneficial for the reduction of carbon and sulfur deposition as long as the catalyst is uniformly distributed with small particle size. For this reason, polishing of the surface of the

anode after catalyst impregnation is not recommendable. Using TiO_2 nanoparticles is a good method to have acceptable particle size distribution but this size can be further improved by adjusting the pH to the isoelectric point during the synthesis to avoid agglomeration of the nanoparticles.

Regarding the operating temperature condition for the anode impregnated with the catalyst, it is recommendable not to exceed or operate above 950°C to avoid reaction of vanadium with the $LSB_{10}T$ or YSZ which is detrimental to the performance of the anode. The anode matrix made of $LSB_{10}T$ at YSZ should be sintered at the condition mentioned in this work followed by impregnation or application of the catalyst.

Preparation of the anode by impregnation of $LSB_{10}T$ inside a porous YSZ instead of $LSB_{10}T$ and YSZ solid state reaction and particle mixing may be a good alternative to increase the TPB but more attention should be addressed on the optimization of the impregnation method to get higher amount of $LSB_{10}T$ with nice nanoparticle distribution. If $LSB_{10}T$ exhibits a predominant electronic conductivity rather than a mixed electronic and ionic conductivity, then the impregnation of the perovskite with the current impregnation procedure can be detrimental to the performance and achievement of higher ionic conductivity due to the formation of a layer formed by the $LSB_{10}T$ on the anode matrix blocking the normal migration of the oxide ions.

Finally, what is certain is that sour gas might have a potential application as fuel for SOFC, as long as the anode is tolerant to sulfur and has the beneficial

effect of H_2S by weather reforming of methane and reduction of carbon and sulfur deposition or the resulting enhancement of catalytic activity or oxidation of methane to produce more electro active gases. More studies are required to determine mechanisms of H_2S involvement in the electrochemical oxidation of methane.